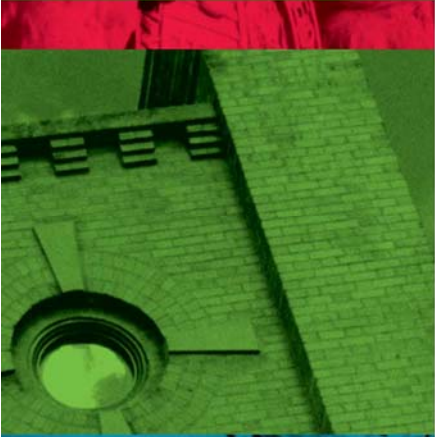




MISSOURI
S&T

CENTER FOR INFRASTRUCTURE ENGINEERING STUDIES



ALKALI-RESISTANT CALCIUM IRON PHOSPHATE GLASS FIBERS FOR CONCRETE REINFORCEMENT

by

Richard K. Brow



**UTC
R129**

**A University Transportation Center Program
at Missouri University of Science & Technology**

Disclaimer

The contents of this report reflect the views of the author(s), who are responsible for the facts and the accuracy of information presented herein. This document is disseminated under the sponsorship of the Department of Transportation, University Transportation Centers Program and the Center for Infrastructure Engineering Studies UTC program at the University of Missouri - Rolla, in the interest of information exchange. The U.S. Government and Center for Infrastructure Engineering Studies assumes no liability for the contents or use thereof.

Technical Report Documentation Page

1. Report No. UTC R129	2. Government Accession No.	3. Recipient's Catalog No.	
4. Title and Subtitle ALKALI-RESISTANT CALCIUM IRON PHOSPHATE GLASS FIBERS FOR CONCRETE REINFORCEMENT		5. Report Date February 2008	
		6. Performing Organization Code	
7. Author/s Richard K. Brow		8. Performing Organization Report No. 00001341	
9. Performing Organization Name and Address Center for Infrastructure Engineering Studies/UTC program Missouri University of Science & Technology 223 Engineering Research Lab Rolla, MO 65409		10. Work Unit No. (TRAIS)	
		11. Contract or Grant No. DTRS98-G-0021	
12. Sponsoring Organization Name and Address U.S. Department of Transportation Research and Special Programs Administration 400 7 th Street, SW Washington, DC 20590-0001		13. Type of Report and Period Covered Final	
		14. Sponsoring Agency Code	
15. Supplementary Notes			
16. Abstract The physical properties and alkaline corrosion resistant properties of calcium-ironphosphate glasses were studied. Iron addition decreases the thermal expansion coefficient and increases the Young's modulus in comparison with the addition of calcium oxide. Glass dissolution behavior in alkaline solutions was studied by weight loss experiments, x-ray diffraction, and analytical scanning electron microscopy. The results show that the dissolution rate decreases when the phosphate chain length decreases. Calcium oxide can improve the glass durability in high pH solutions in comparison with ferric oxide. Phase equilibrium modeling was used to explain the formation of corrosion products, including hydroxyapatite.			
17. Key Words Construction materials; reinforced cement.	18. Distribution Statement No restrictions. This document is available to the public through the National Technical Information Service, Springfield, Virginia 22161.		
19. Security Classification (of this report) unclassified	20. Security Classification (of this page) unclassified	21. No. Of Pages 61	22. Price

UTC FINAL REPORT

(For the Period October 1, 2004 to September 30, 2007)

**ALKALI-RESISTANT CALCIUM IRON PHOSPHATE GLASS FIBERS FOR
CONCRETE REINFORCEMENT**

submitted by:

Richard K. Brow

Missouri University of Science & Technology

Department of Materials Science & Technology

110 Straumanis Hall, Rolla, MO 65409

(573) 341-6812; (573) 341-2071 fax; brow@mst.edu

January 31, 2008

Executive Summary

Funds from the University Transportation Center (UTC) were leveraged with those received from the US Department of Energy (OIT/DOE Award DE-FC36-04GO14046), through a sub-contract with Mo-Sci Corporation (Rolla, MO), to support the development of alkaline-resistant phosphate glass fibers for reinforcing cement composites. The research resulted in two Master's theses, a patent application, and a number of presentations and publications by the students involved.

Over 20 glasses were prepared and evaluated by students supported by UTC, and over 280 glasses were prepared and evaluated in the overall program. Alkaline-resistant phosphate compositions were identified, but fibers drawn from these melts did not offer any mechanical advantage over current state-of-the-art silicate-based alkaline resistant glass fibers for reinforcing cement composites. The corrosion reactions between glasses and alkaline solutions were studied in detail, and the conversion of the glass surfaces to hydroxyapatite was seen as responsible for the poor mechanical properties of the composites. Other applications for new corrosion-resistant glasses are under development at Mo-Sci Corp.

This report is divided into three sections, representing the work done by the two students who were supported by UTC funds. The first section reviews research on glass corrosion in alkaline solutions, done by Ms. Jiawanjun Shi as part of her requirements for a Master's degree in the Materials Science & Engineering Department. The second section reviews the mechanical testing of fiber-reinforced cement composites and the third section reviews the corrosion of glass fibers in cement environments. Both studies were done by Ms. Rossella Ferraro, as part of her requirements for a Master's degree in the Civil and Architectural Engineering Department.

Section 1

PROPERTIES OF ALKALINE-RESISTANT CALCIUM-IRON-PHOSPHATE GLASSES

Jiawanjun Shi and Richard K. Brow
Materials Science & Engineering Department

ABSTRACT

The physical properties and alkaline corrosion resistant properties of calcium-iron-phosphate glasses were studied. Iron addition decreases the thermal expansion coefficient and increases the Young's modulus in comparison with the addition of calcium oxide. Glass dissolution behavior in alkaline solutions was studied by weight loss experiments, x-ray diffraction, and analytical scanning electron microscopy. The results show that the dissolution rate decreases when the phosphate chain length decreases. Calcium oxide can improve the glass durability in high pH solutions in comparison with ferric oxide. Phase equilibrium modeling was used to explain the formation of corrosion products, including hydroxyapatite.

1. INTRODUCTION

Glass fiber-reinforced cement composites have been used for nonstructural building materials since the early 1970s [1]. In general, the fibers greatly increase the flexural strength of composites relative to unreinforced cement. However, glass fiber-reinforced cement composites tend to lose strength as a result of the reaction between the highly alkaline cement matrix and the glass fibers [2].

The recent discovery of iron phosphate glasses with low melting temperatures (between 1100°C to 1200°C), outstanding corrosion resistance and continuous fiber pulling ability has attracted much interest [3-4]. However, the main challenge phosphate glasses face for the cement reinforcement application is to improve the chemical durability in high pH conditions. Researchers found that some phosphate glass compositions can be made to be highly durable [5]. The main concern of this project is to study the properties of calcium-iron-phosphate glasses and the corrosion mechanism of the phosphate glasses in cement environments.

CORROSION STUDIES OF CEMENT REINFORCEMENT GLASS FIBERS

The cement porewater environment is typically a highly alkaline environment. Ordinary cement consists of calcium oxide, silicon oxide and smaller quantities of aluminum, iron, magnesium, and potassium oxides. Upon hydration, the cement hardens into its gel phase with by-products of calcium hydroxide, sodium hydroxide and potassium hydroxide [6]. These hydroxides remain in solution with the concrete porewater and contribute to the high pH of the porewater [7].

The decomposition of silicate glasses in high pH aqueous environment has been studied by a number of investigators [5, 8-11]. These studies reveal that most silicate glasses are decomposed at pH>10 [8]. Budd suggested that the polarity of the strong siloxane bond and the positive charge residing on the silicon atom makes the bond susceptible to attack by hydroxyl ions.

Scarinci et al. found that the formation of an adherent surface layer of reaction product can act as a protective coating and decrease the rate of further corrosion [10]. Therefore the

relative permeability of the coating towards the diffusion of ionic species would become the rate determining step in hindering further corrosion. As for alkaline resistant (AR) glass fibers, the addition of ZrO_2 increases the corrosion resistance of glass immersed in cement environment by forming a thin, stable, passivating layer on the surface. However, this layer cannot prevent further depletion of SiO_2 and the penetration of hydroxyl ions [11]. Yilmaz et al. suggested that the corrosion of AR glass in a NaOH solution proceeds in three steps: dissolution of glass and formation of Zr-rich insoluble layer; further but slower dissolution of glass and thickening of Zr-rich layer; cracking in the layer and attack on new glass surface [8].

Corrosion Studies of Phosphate Glass.

The rate of phosphate glass dissolution is dependent on the glass composition [12]. The overall dissolution processes include acid/base reactions, hydrolysis reactions and hydration reactions.

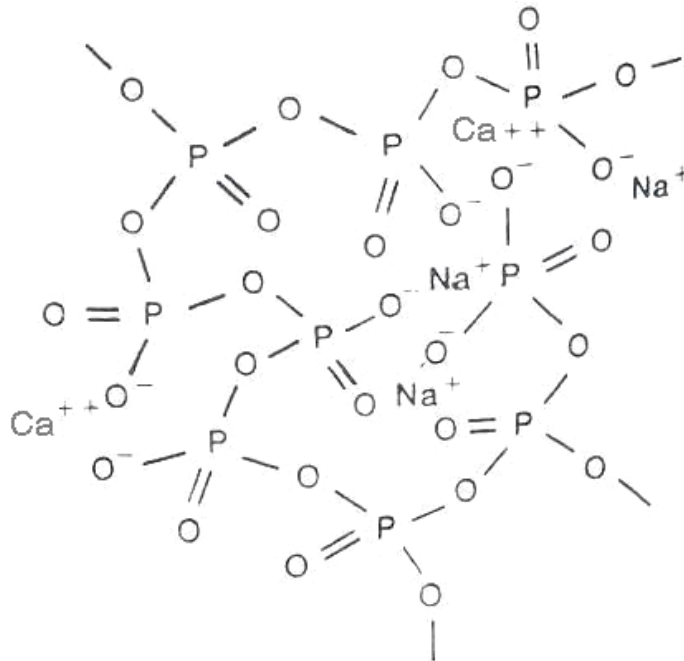
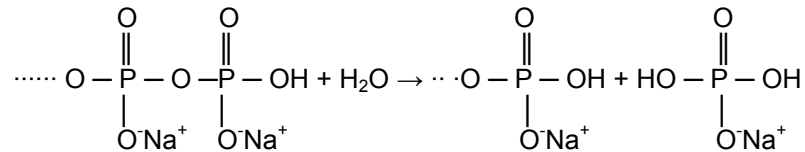


Figure 1.1. The structure of Na-Ca-phosphate glass [12].

The hydrolysis reaction can be expressed as follows [12]:



P-O-P bonds break up, and produce orthophosphate anions that are released into the solution [12]. However, the hydrolysis reactions only accelerate in acidic not in basic solutions. P-O-P bonds in linear phosphate chains are known to be as resistant to hydrolysis as Si-O-Si bonds in neutral pH solutions [13].

Bae et al. studied the effect of amount of P₂O₅ on the glass dissolution [13]. They showed that the branching Q³ phosphate tetrahedra can serve as steric hindrance to the diffusion of water into the glass and consequently lower the dissolution rate. However, strain is also introduced into the network and encourages the hydrolytic scission of the branching units. Hence, high P₂O₅ content and long Q² chains improve the glass durability. They also found that in alkaline solutions, the glass dissolves non-uniformly, preferentially releasing phosphate anions.

Cacaina et al. concluded that the formation of a surface layer in solution plays an important role in the glass dissolution process [14]. The surface reaction product may have a similar network molecular structure as the original glass except the modifier ions have been replaced by a hydrogen ion plus one or more water molecules. The other possibility is the layer transforms over time by localized hydrolysis and condensation reactions into a gel layer.

Hydration reactions occur at modifier cations, disrupting ionic bonds between the phosphate chains.

A useful approach to improve the chemical durability of phosphate glass is to add various oxides [15]. Feng et al. built a model to quantify the relationship between glass compositions and their chemical durability [16]. They assumed the strengths of the bonds between cations and oxygens and the structural roles of the individual elements in the glass are the predominant factors in the composition dependence of the glass chemical durability. The order of increasing effectiveness is expressed as Al₂O₃> B₂O₃>ZrO₂> SiO₂>Fe₂O₃> CaO.

Many researchers found the addition of iron will improve durability for phosphate glass [13, 15-21]. Several researchers concluded that Fe³⁺ cations can enter in the glass network with

four-fold coordination and form stable P-O-Fe covalent bonds and consequently increase the chemical durability [17,18]. Yu et al. studied the relationship between iron valence and the ability of iron addition to improve glass durability [15].

Bunker et al. suggested that divalent cations like Ca^{2+} can serve as ionic cross-links between the nonbridging oxygens of two different phosphate chains, and accordingly increase chemical durability. On the other hand, when divalent cation content reaches a certain point, because the polymer chains can only accommodate a limited number of chelate cross links, there is no further improvement in chemical durability [12].

SUMMARY AND THESIS STATEMENT

Low cost and superior properties have made phosphate glass a good candidate for cement reinforcement applications. The biggest challenges are to know how phosphate glass reacts in cement environment and then to improve the chemical durability. Many researchers have studied the corrosion mechanism of phosphate glasses in neutral solution, but very few have done these studies in high alkaline environments. This research explores this new area and tries to answer questions about how phosphate glasses react in alkaline environments. From the previous result of compositional effects on phosphate glass structure and properties, both ferric oxide and calcium oxide can improve the chemical durability. This project will continue the study of the composition effects and do the comparison. Also, the effect of different phosphate chain-lengths on the glass durability will be discussed.

2. EXPERIMENTAL PROCEDURES

SAMPLE PREPARATION

Glasses were prepared from reagent grade CaCO_3 , Fe_2O_3 , and $\text{NH}_4\text{H}_2\text{PO}_4$ (Fisher Scientific Inc.). All components were weighed on a balance that provided measurements accurate to $\pm 0.01\text{g}$. Components were mixed thoroughly in aluminosilicate crucibles, and then preheated at 900°C for 1 hour in order to volatilize NH_3 and CO_2 . The batch materials were then melted at 1200°C for 2 hours. Melts were poured into copper molds and the glasses annealed at 450°C for

6 hours. Samples for corrosion studies were cut with a diamond saw to dimensions about $0.5 \times 1 \times 2 \text{ cm}^3$, then polished to 600 grit finish with SiC paper on all surfaces; water was used as a lubricant.

Samples of each glass were ground using a mortar and pestle and sieved to produce powders with particle sizes in the range of approximately 125-150 μm . These particles were used for accelerated corrosion tests.

Glass fibers were pulled from melts to produce samples for measuring Young's modulus. Melts were held in aluminosilicate crucibles at 1300°C for one hour, and then removed from the furnace. A silica rod was used to pull fibers from the melt surface. The glass fiber diameters were around $200 \mu\text{m}$.

Table 2.1 shows the batched compositions of glasses prepared in this study. The glasses are classified according to their O/P atom ratio, thus falling into three compositional groups: metaphosphate (O/P=3.0), polyphosphate (O/P=3.25), and pyrophosphate (O/P=3.5) glasses.

PHYSICAL PROPERTIES CHARACTERIZATION

Physical property measurements on glass samples included density (ρ), coefficients of thermal expansion (CTE), and Young's modulus. Glass density was determined by the Archimedes method using DI water as the buoyancy liquid. Density was measured on two samples for each composition, with an uncertainty of $\pm 0.003 \text{ g/cm}^3$. Thermal expansion coefficient was measured in air using an Orton 1600 dilatometer at a ramp rate of $5^\circ\text{C}/\text{min}$. The linear CTE was calculated from the length change between 100°C to 500°C for each glass. The CTE of a glass run twice varied by 5%. The glass transition temperature (T_g) and dilatometric softening temperatures (T_d) were determined from the dilatometry results. They are reproducible to $\pm 3^\circ\text{C}$. Young's modulus was measured on fibers pulled from each melt using an ultrasonic acoustic pulse technique, (Panatherm 5010, Panametrics, Inc., Waltham, Massachusetts). Ten different fibers drawn from melts of each composition were analyzed and the average modulus is reported.

Table 2.1. Batched Compositions (mole %) of $\text{CaO-Fe}_2\text{O}_3\text{-P}_2\text{O}_5$ Glasses

ID	O/P	CaO	Fe ₂ O ₃	P ₂ O ₅	CaO/P ₂ O ₅	Fe ₂ O ₃ /P ₂ O ₅	CaO/(Fe ₂ O ₃ +CaO)
CFP01	3.0	50.00	0.00	50.00	1.00	0.00	1.00
CFP02		30.00	10.00	60.00	0.50	0.17	0.75
CFP03		16.70	16.70	66.60	0.25	0.25	0.50
CFP04		0.00	25.00	75.00	0.00	0.33	0.00
CFP05		40.91	4.55	54.55	0.75	0.08	0.90
CFP06		35.71	7.14	57.14	0.63	0.13	0.83
CFP07		21.43	14.29	64.29	0.33	0.22	0.60
CFP21	3.25	60.00	0.00	40.00	1.50	0.00	1.00
CFP22		37.50	12.50	50.00	0.75	0.25	0.75
CFP23		27.30	18.20	54.50	0.50	0.33	0.60
CFP24		0.00	33.00	67.00	0.00	0.50	0.00
CFP25		46.00	8.00	46.00	1.00	0.17	0.85
CFP26		15.00	25.00	60.00	0.25	0.42	0.38
CFP27		44.12	8.82	47.06	0.94	0.19	0.83
CFP28		21.43	21.43	57.14	0.38	0.38	0.50
CFP51	3.5	66.70	0.00	33.30	2.00	0.00	1.00
CFP52		50.00	10.00	40.00	1.25	0.25	0.83
CFP53		25.00	25.00	50.00	0.50	0.50	0.50
CFP54		0.00	40.00	60.00	0.00	0.67	0.00
CFP55		43.00	14.00	43.00	1.00	0.33	0.75
CFP56		35.00	19.00	46.00	0.76	0.41	0.65
CFP57		14.00	32.00	55.00	0.25	0.58	0.30
CFP58		31.58	21.05	47.37	0.67	0.44	0.60

CHEMICAL DURABILITY TESTS

Dissolution rates were measured gravimetrically on monolithic samples (two samples for each glass composition) held in Lawrence solution (LS) at 80°C for up to 1000 hours. Lawrence solution is prepared from 0.88 g/l NaOH, 3.45 g/l KOH, and 0.48 g/l Ca(OH)₂ suspended in distilled water and has a pH of approximately 13.0. It is used as a synthetic cementitious environment [21]. The glass surface area-to-solution volume ratios were set to 0.07cm⁻¹. Glass powders were suspended in NaOH solution (pH=13, 0.1 molar/L) from 2 hours up to 20 hours at 80°C and the glass surface area-to-solution volume ratios were set to 0.21cm⁻¹. Weight change measurements were made using a Sartorius scale with 10⁻⁵g resolution. The solution temperatures were maintained at 80°C to accelerate the reaction with the glass. The dissolution rates were obtained by dividing the weight loss by the surface areas and the immersion time. The pH values of the solutions were measured by the Accumet pH meter AR25. For accuracy, each dissolution experiment was repeated.

SAMPLE CHARACTERIZATION

The crystal phases of as-made glasses and corroded glasses were examined by a Scintag LET2400 X-ray diffractometer. The step rate was 0.03deg/sec and the angles scanned were 3° to 90°2θ. Both bulk glasses and powders were examined by XRD before and after corrosion tests.

Scanning Electron Microscopic (SEM) images were taken using the Hitachi S4700 on glass samples before and after corrosion. Standardless energy dispersive spectroscopic (EDS) analyses were performed using EDAX S-4700 ($V_{acc}=15kV$).

3. RESULTS

GLASS AND FIBER FORMATION

Figure 3.1 summarizes the glass forming tendencies of the compositions studied. Compositions of polyphosphate and pyrophosphate glasses containing between 40 to 60 mol% CaO were partially crystallized on their surface, whereas compositions containing more than 60 mol% were heavily crystallized. X-ray diffraction analyses (Figure 3.2) revealed that Ca₂P₂O₇

crystals form in the CaO-rich samples; all other compositions are amorphous, including glasses with high Fe_2O_3 contents.

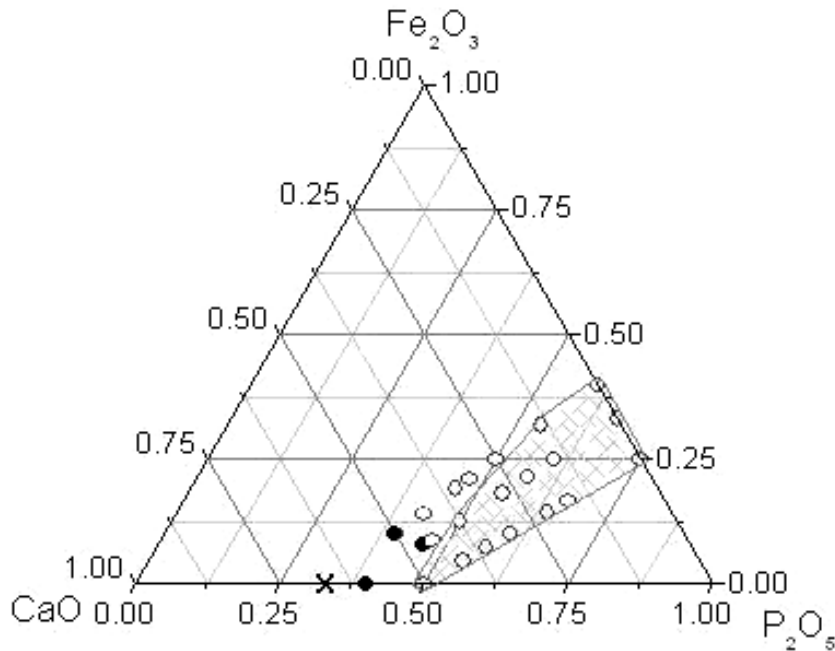


Figure 3.1. Composition and glass forming ability of calcium iron phosphate glasses. Open circles indicate compositions that formed bulk glasses, closed circles represent partially crystallized compositions, and crosses represent heavily crystallized compositions. The cross-hatched area represents compositions for which fibers could be drawn from melt surface.

Several compositions that produce bulk glasses would not produce glass fibers from melts held at 1300°C . Fibers could be pulled from all metaphosphate ($\text{O/P}=3.00$) melts at 1300°C , but polyphosphates ($\text{O/P}=3.25$) with CaO content ≥ 50 mol% and pyrophosphates ($\text{O/P}=3.50$) with more than 14 mol% CaO did not produce homogeneous glass fibers. The cross-hatched area in Figure 3.1 shows the fiber pulling range.

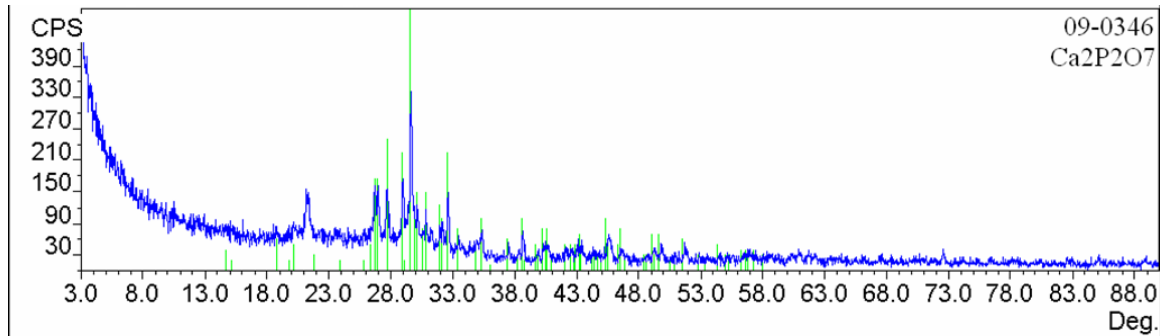


Figure 3.2. XRD pattern of the as-made CFP52 glass showing the presence of $\text{Ca}_2\text{P}_2\text{O}_7$ crystals

PHYSICAL PROPERTIES

Table 3.1 summarizes the physical properties that were determined for the three series of $\text{CaO-Fe}_2\text{O}_3\text{-P}_2\text{O}_5$ glasses. Comparisons are made with the reported properties of several glasses [22]. In general, density (Figure 3.3) and Young's modulus (Figure 3.4) both decrease as CaO replaces Fe_2O_3 in each compositional series. In addition, the density and Young's modulus of the glasses increase in the order metaphosphates < polyphosphates < pyrophosphates.

The coefficients of thermal expansion decrease as Fe_2O_3 replace CaO (Figure 3.5). In general, the metaphosphate glasses have the lower CTE's and the pyrophosphates have the greater CTE's.

Table 3.1. Properties of Calcium Iron Phosphate Glasses

ID	Composition molar%			Density g/cm ³	T _g °C	T _s °C	CTE 10 ⁻⁶ /°C	Young's modulus/GPa
	CaO	Fe ₂ O ₃	P ₂ O ₅					
CFP-01	50.00	0.00	50.00	2.643±0.003	565	596	11.20	53.87±1.03
CP50[22]	50.00	0.00	50.00	2.71	550	NM	10.00	NM
CFP-06	35.71	7.14	57.14	2.694±0.001	546	602	10.10	NM
CFP-02	30.00	10.00	60.00	2.723±0.001	535	567	9.87	57.87±1.16
CFP-07	21.43	14.29	64.29	2.730±0.001	NM	NM	NM	NM
CFP-03	17.00	17.00	66.00	2.769±0.002	545	585	8.84	62.24±2.20
CFP-04	0.00	25.00	75.00	2.822±0.001	550	601	7.91	64.90±1.46
CFP-21	60.00	0.00	40.00	2.787±0.013	NM	NM	NM	NM
CFP-25	46.00	8.00	46.00	2.851±0.008	NM	NM	NM	NM
CFP-22	37.00	13.00	50.00	2.898±0.001	520	561	10.20	64.85±2.65
CFP-23	27.00	18.00	55.00	2.925±0.001	520	573	9.44	66.95±1.07
CFP-26	15.00	25.00	60.00	2.932±0.003	505	550	9.10	NM
CFP-24	0.00	33.00	67.00	2.949±0.003	515	550	8.22	66.35±0.93
CFP-52	50.00	10.00	40.00	3.000±0.002	NM	NM	NM	NM
CFP-55	43.00	14.00	43.00	3.041±0.003	NM	NM	NM	NM
CFP-58	31.58	21.05	47.37	3.042±0.001	529	569	10.20	NM
CFP-56	35.00	19.00	46.00	3.075±0.001	NM	NM	NM	NM
CFP-53	25.00	25.00	50.00	3.075±0.001	527	560	10.20	NM
CFP-57	14.00	32.00	55.00	3.095±0.010	503	545	8.93	NM
CFP-54	0.00	40.00	60.00	3.085±0.005	499	519	9.08	66.84±1.48
FP40[22]	0.00	40.00	60.00	3.04	502	NM	7.70	NM

NM---not measured.

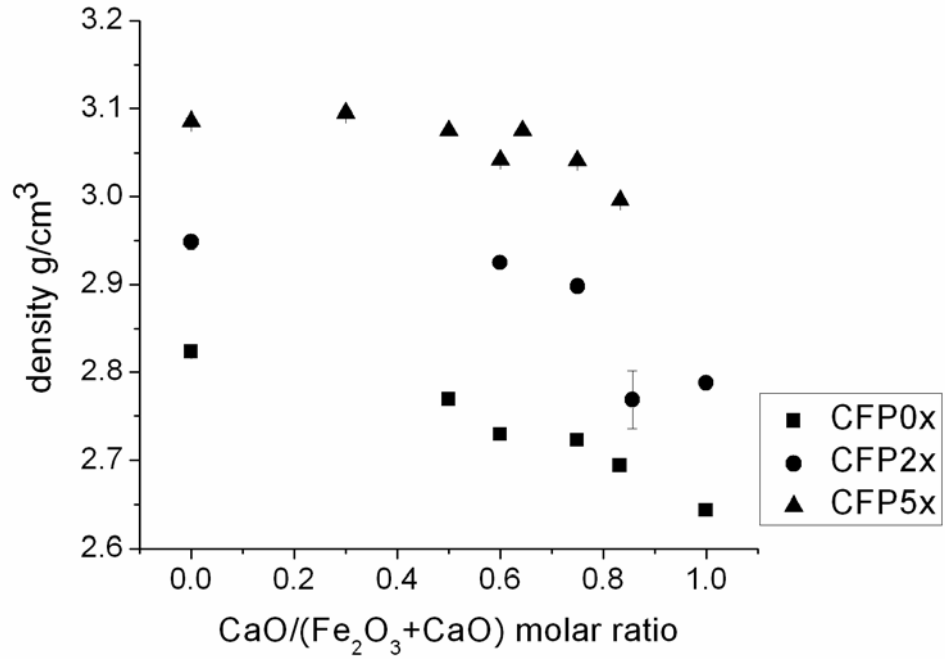


Figure 3.3. Density of calcium iron phosphate glasses

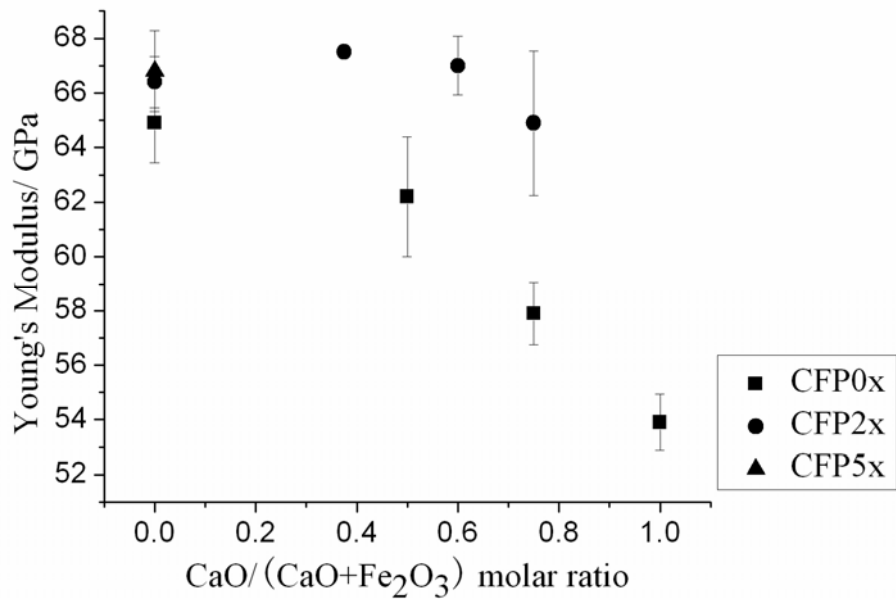


Figure 3.4. Young's modulus of calcium iron phosphate glasses

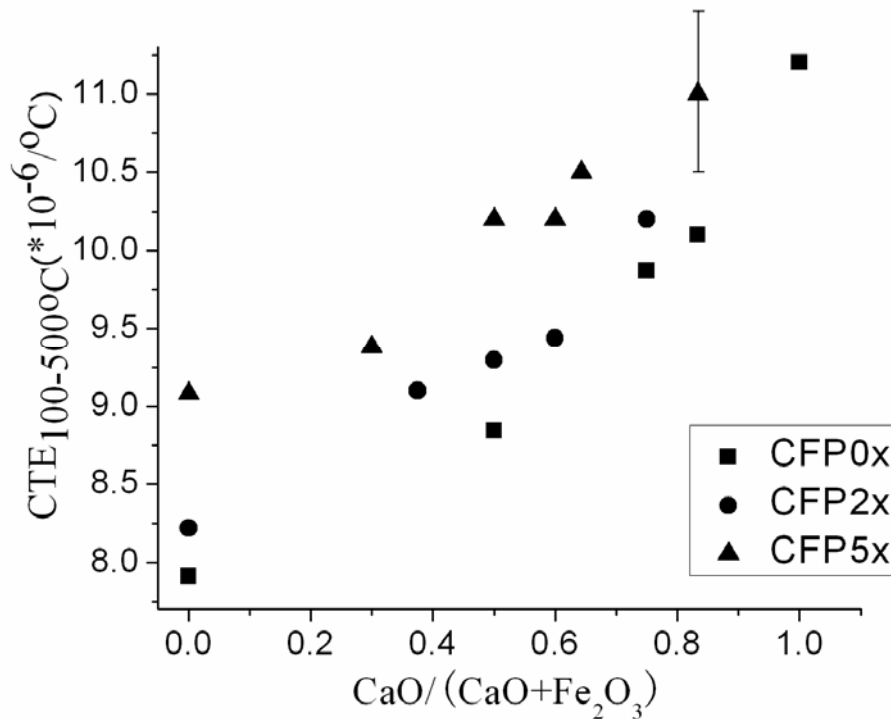


Figure 3.5. Average thermal expansion coefficient between 100°C and 500°C for calcium iron phosphate glasses

CORROSION BEHAVIOR

Figures 3.6-3.8 show the weight losses in Lawrence solution of glass monoliths versus time for the three compositional series at 80°C. In general, the initial corrosion rate is high, but decreases with time after ~200 hours. For most compositions, the glass weight does not change much after 500 hours. CFP01 (Fe-free Ca-metaphosphate) disintegrates after 500 hours and the other bulk samples stayed intact after up to 1000 hours.

The pH of Lawrence solution decreases as the phosphate glasses react, as shown in Figures 3.9 – 3.11. The extent of the pH decrease depends on the O/P molar ratio of the glasses. The metaphosphate glasses caused the greatest decrease of pH, to values from ~4 (for the iron-free glass) to ~7 (for the calcium-free glass). The final pH values (after 1000 hours) for the corroded poly- and pyrophosphate series ranged from 7 to 13. Glasses with greater CaO-contents produced less change in solution pH, except for the CFP01 glass.

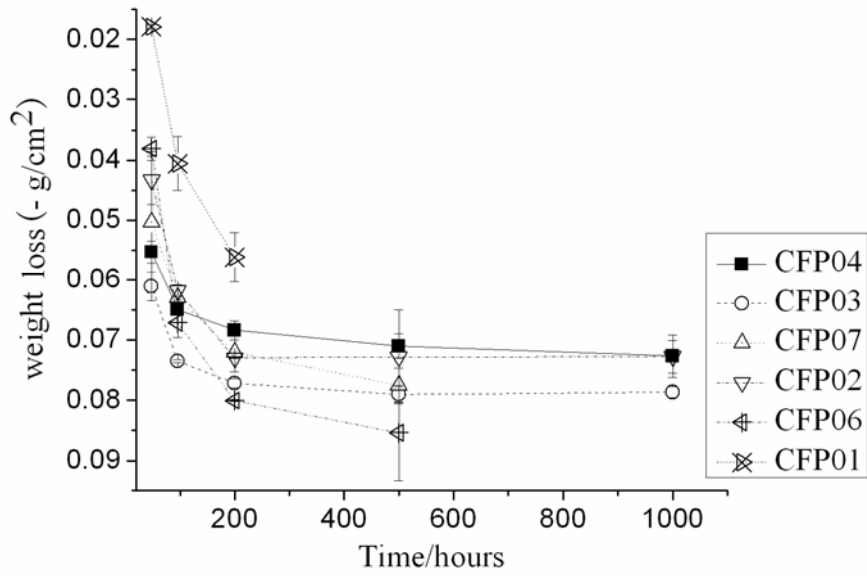


Figure 3.6. Weight loss of Ca-Fe-metaphosphate (O/P=3.00) glasses in LS at 80°C

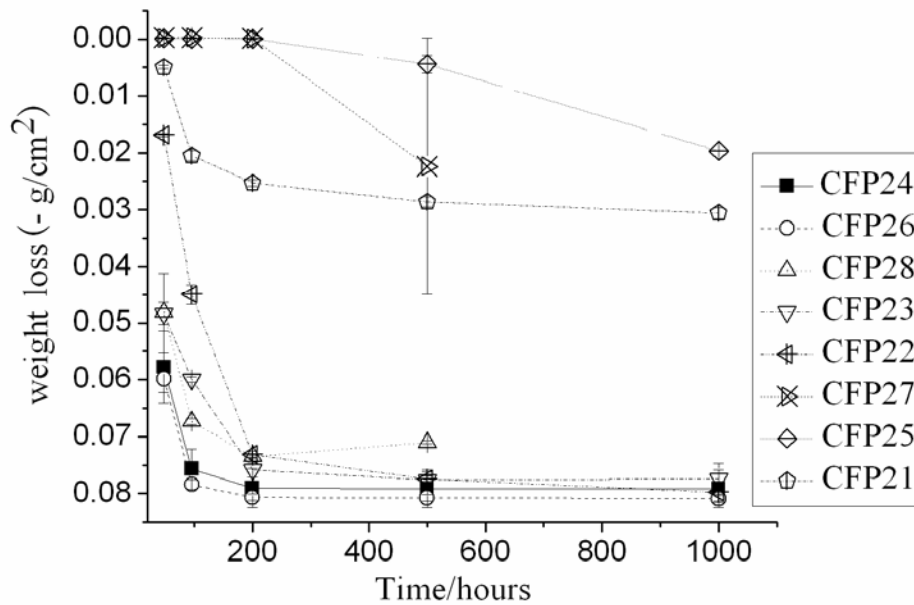


Figure 3.7. Weight loss of Ca-Fe-polyphosphate (O/P=3.25) glasses in LS at 80°C

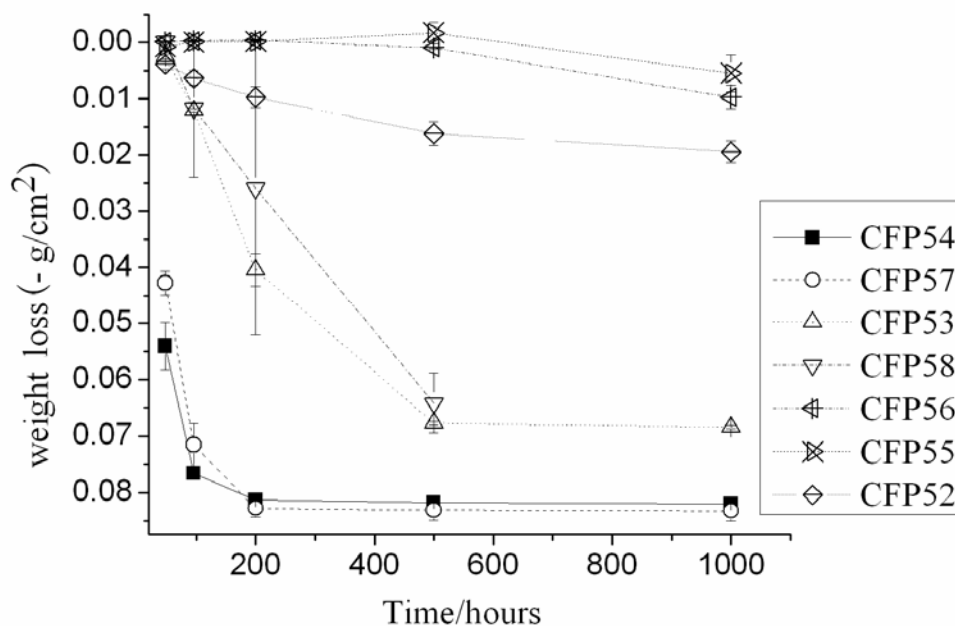


Figure 3.8. Weight loss of Ca-Fe-pyrophosphate (O/P=3.5) glasses in LS at 80°C

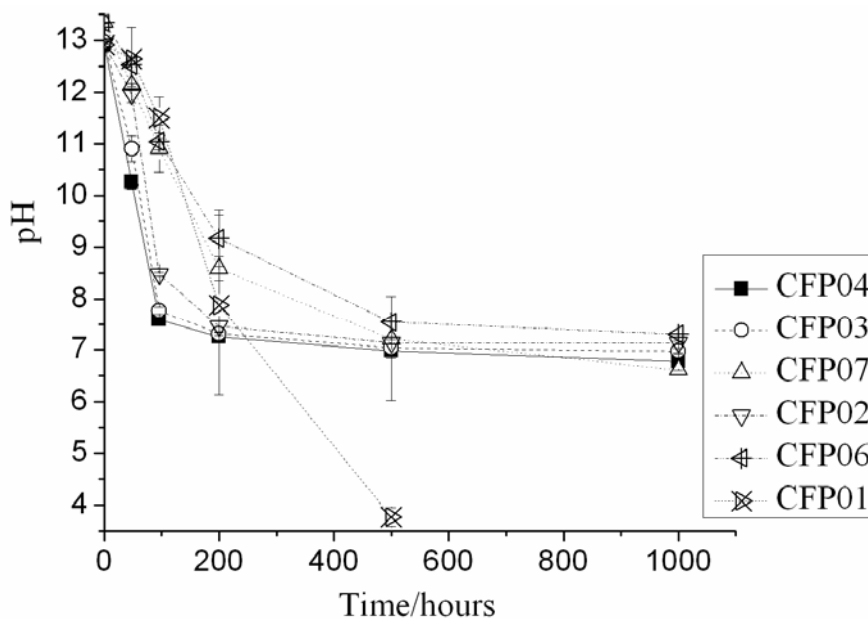


Figure 3.9. Change of Lawrence solution pH during corrosion tests of Ca-Fe-metaphosphate (O/P=3.00) glasses at 80°C

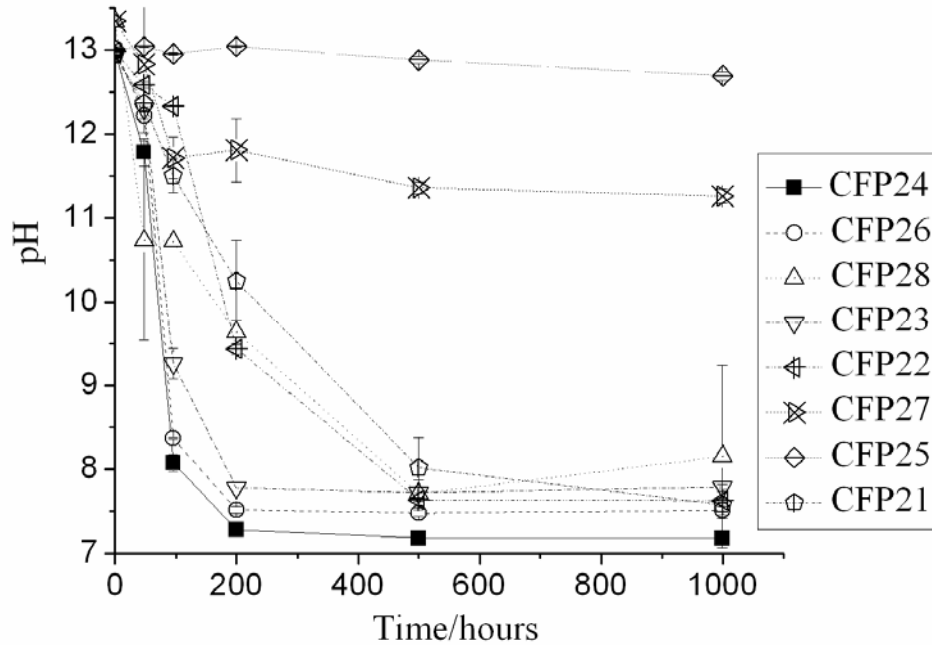


Figure 3.10. Change of Lawrence solution pH during corrosion tests of Ca-Fe-polyphosphate (O/P=3.00) glasses at 80°C

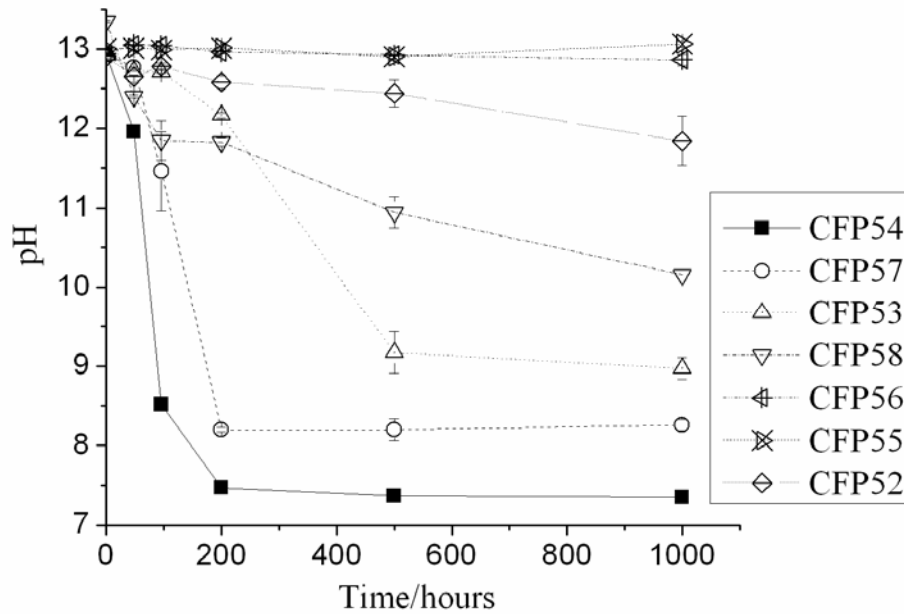


Figure 3.11. Change of Lawrence solution pH during corrosion tests of Ca-Fe-pyrophosphate (O/P=3.00) glasses at 80°C

After corrosion in LS solution for 500 hours at 80°C, CFP01 glass disintegrated and formed CaHPO_4 crystals (Figure 3.12); other glass compositions formed small amounts of $\text{Ca}_5(\text{PO}_4)_3\text{OH}$ crystals (Figure 3.13), except for CFP04 which remained amorphous.

Polyphosphate glasses with 21mol% to 44mol% CaO and pyrophosphate with 25mol% to 32mol% CaO also formed small amount of $\text{Ca}_5(\text{PO}_4)_3\text{OH}$ crystals on their corroded surfaces. CFP21 and CFP52 glasses still have $\text{Ca}_2\text{P}_2\text{O}_7$ crystals on their surface after exposure to Lawrence solutions, and the intensity of the XRD peak is greater than what was formed for the “as-made” glass (Figure 3.2). The XRD analyses of corroded surfaces are summarized in figure 3.14.

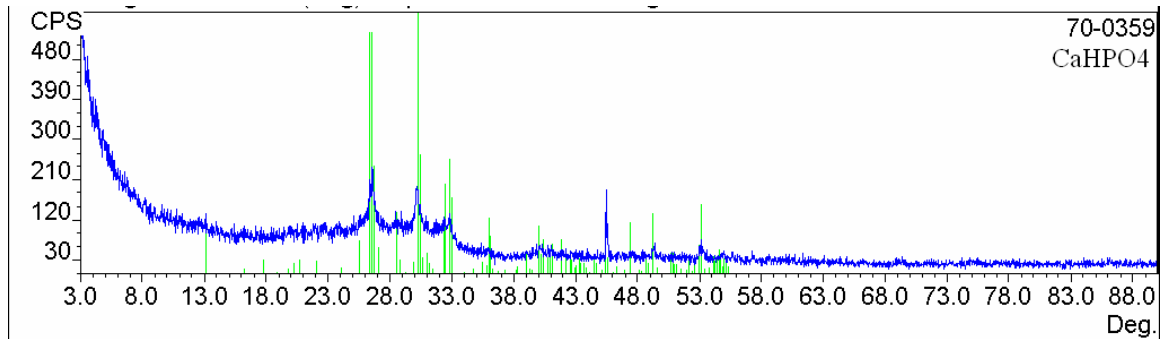


Figure 3.12. XRD analyses of CFP01 glass after corrosion in LS at 80°C for 500 hours

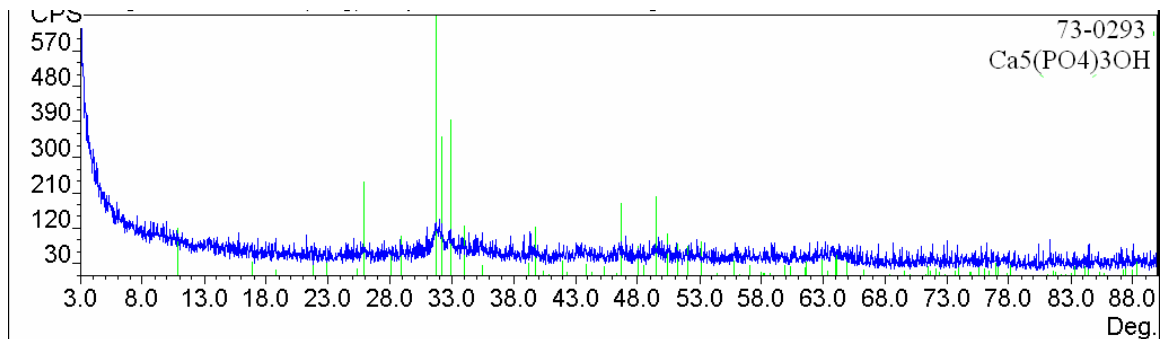


Figure 3.13. XRD analyses of CFP58 glass after corrosion in LS at 80°C for 500 hours

SEM images of the surfaces of selected compositions after LS corrosion tests for 500 hours are shown in Figure 3.15 – 3.18. The surface of the metaphosphate glass CFP03 is covered by a thick reaction product (Figure 3.15). Pyrophosphate CFP27 surfaces have a different appearance (Figure 3.16). The surface of the high iron oxide content pyrophosphate CFP53 is crowded with small particles (Figure 3.17), whereas the CFP55 surface seems to be selectively attacked (Figure 3.18).

EDS spectra were collected on each surface area and these results are summarized in Table 3.2. For the metaphosphate CFP03, both Ca/P and Fe/P atom ratios increase when the

corroded surface is compared to the “as-made” (unreacted) surface. For the polyphosphate CFP27 and for the pyrophosphate CFP55, the Ca/P ratios on the corroded surfaces are greater than on the “as-made” surfaces, whereas the Fe/P ratio on the surface of the “high Fe₂O₃” pyrophosphate CFP53 is increased after corrosion.

Table 3.2. EDS analyses from as-made glass surfaces and corroded glass surfaces (after 500 hours in LS)

ID	Batched composition atom ratios		Unreacted surface atom ratios		Reacted surface atom ratios	
	Fe/P	Ca/P	Fe/P	Ca/P	Fe/P	Ca/P
CFP03	0.25	0.13	0.28±0.01	0.12±0.02	0.43±0.01	0.25±0.01
CFP27	0.19	0.47	0.20±0.02	0.45±0.04	0.22±0.05	1.04±0.12
CFP53	0.50	0.25	0.46±0.04	0.23±0.03	0.58±0.05	0.25±0.01
CFP55	0.33	0.50	0.36±0.03	0.50±0.01	0.39±0.03	1.23±0.01

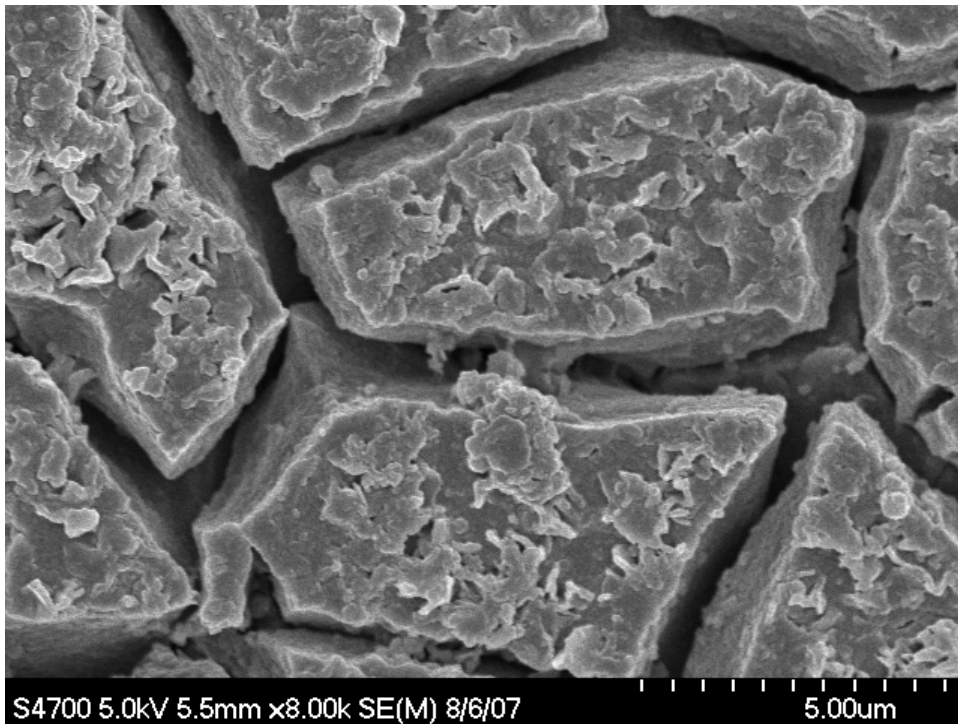


Figure 3.15. SEM image of CFP03 glass surface after corrosion for 500 hours in LS

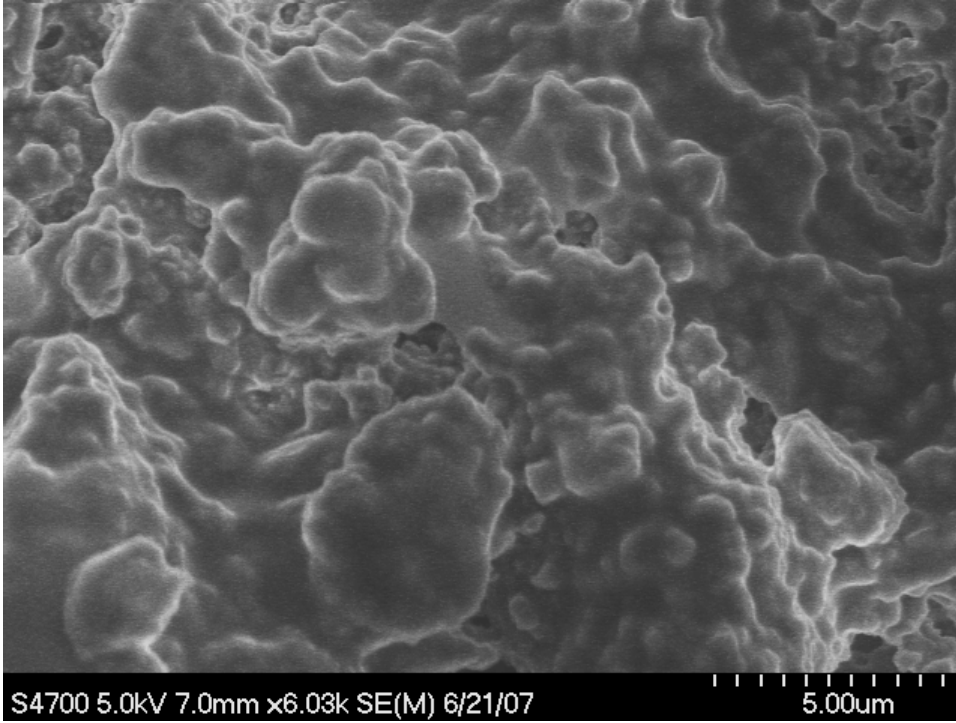


Figure 3.18. SEM image of CFP27 glass surface after corrosion for 500 hours in LS

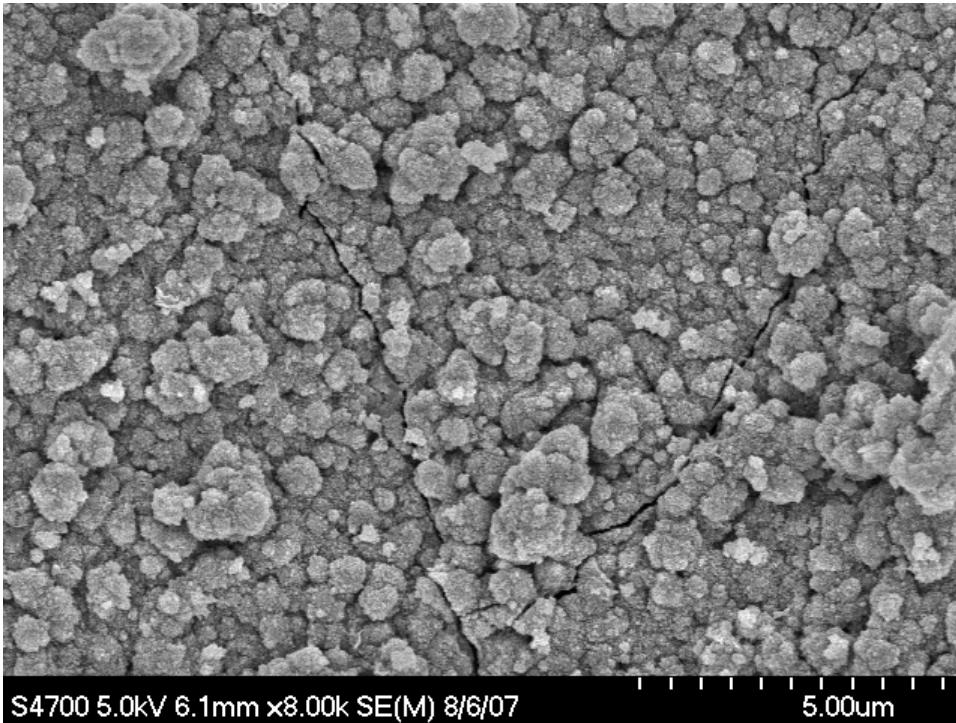


Figure 3.19. SEM image of CFP53 glass surface after corrosion for 500 hours in LS

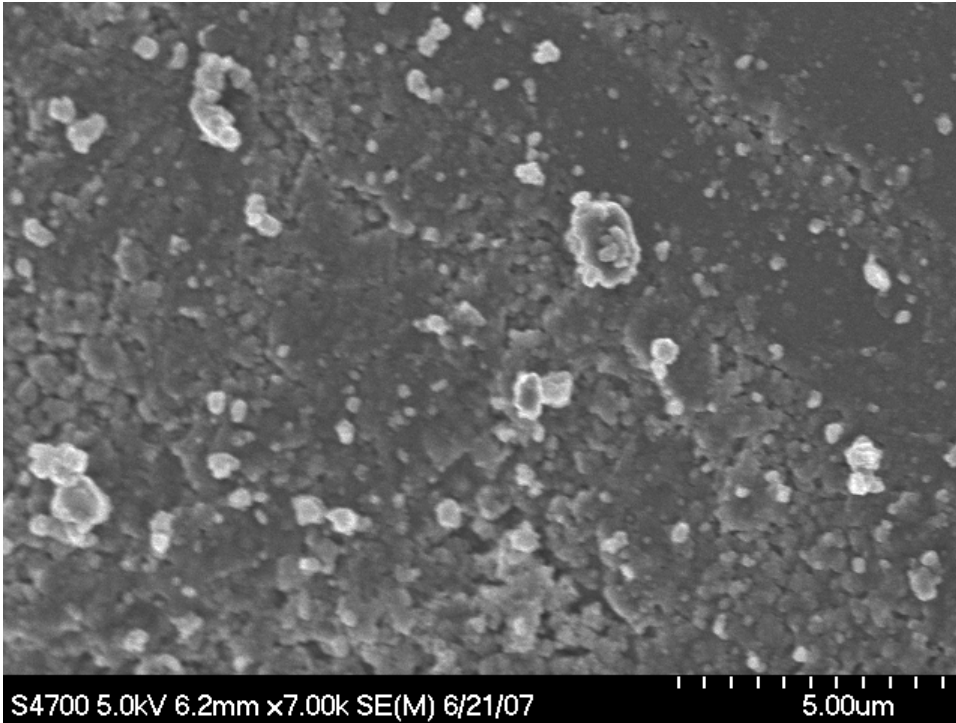


Figure 3.20. SEM image of CFP55 glass surface after corrosion for 500 hours in LS

XRD results of glass powders corroded in NaOH are similar to results obtained by XRD analyses of glass bulk in LS. $\text{Ca}_5(\text{PO}_4)_3\text{OH}$ crystals were detected on most glass surfaces, except for CFP04, CFP24 and CFP54 which formed Fe_2O_3 crystals .

The XRD analyses are summarized in figure 3.14, where the principal crystalline phases identified on each glass surface after 1000 hours in Lawrence solution are indicated.

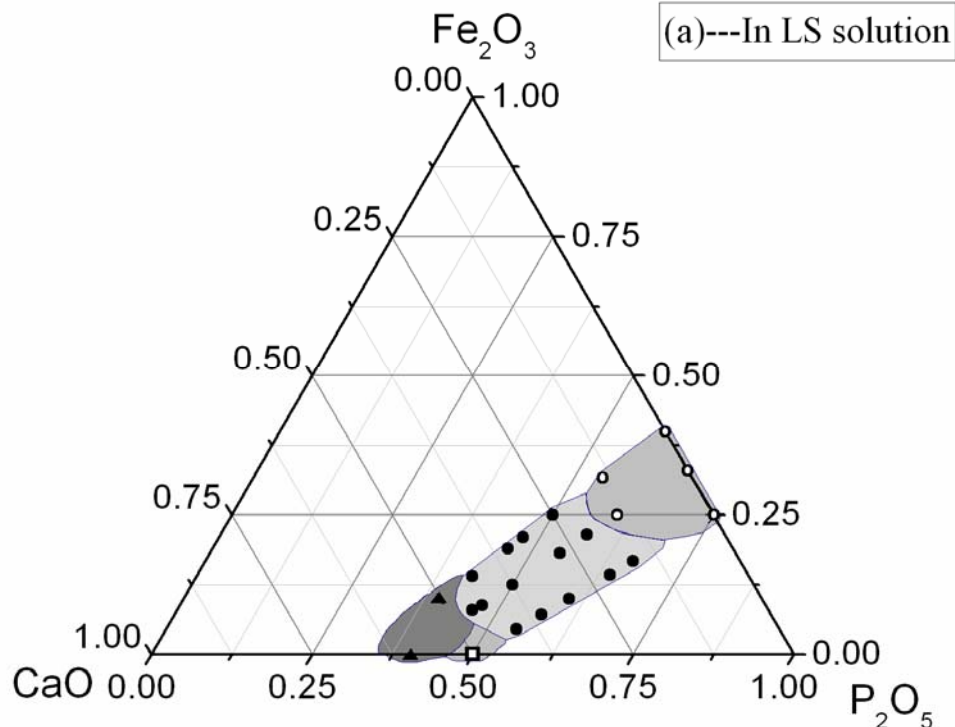


Figure 3.14. Surface corrosion products identified by XRD on glasses exposed to 80°C LS for 1000 Hours. Triangles represent $\text{Ca}_2\text{P}_2\text{O}_7$ crystals; open circles indicate amorphous materials; closed circles indicate $\text{Ca}_5(\text{PO}_4)_3\text{OH}$ crystals; open squares represent CaHPO_4 crystals.

To summarize the corrosion results:

Dissolution rates in alkaline solutions decrease with decreasing phosphate chain length. The glass composition does not make a significant difference for metaphosphate glasses in the form of weight loss and pH change in LS.

CaO additions to polyphosphate and pyrophosphate glasses improve glass durability in LS and NaOH solutions compared with Fe_2O_3 addition.

The corroded surfaces are calcium-rich for high-CaO-content poly- and pyrophosphate glass, but iron-rich for high- Fe_2O_3 -content pyrophosphate glass.

Most compositions form $\text{Ca}_5(\text{PO}_4)_3\text{OH}$ crystals after corrosion in LS and NaOH solutions. Iron-phosphate glasses form Fe_2O_3 crystals after corrosion in NaOH solutions but remain amorphous in LS solutions. Calcium-metaphosphate glass form CaHPO_4 crystal after corrosion in NaOH solutions but form $\text{Ca}_5(\text{PO}_4)_3\text{OH}$ crystals in LS solutions.

4. DISCUSSION

PROPERTIES

Glass Formation

The XRD analyses of bulk samples showed that all of the compositions have good glass forming ability expect for glasses CFP21 and CFP52 which formed $\text{Ca}_2\text{P}_2\text{O}_7$ crystals upon quenching. This confirms Meadowcroft's theory that ease of formation of monovalent and divalent phosphate glasses could be related to the heat of formation of the solid glass [23-24]. Because the heat of formation of iron phosphate (14 kJ/mol-atoms) is lower than that of calcium phosphate (55 kJ/mol-atoms), the iron phosphate chains would distribute more broadly, and Fe_2O_3 -rich glasses would form more easily [23]. In addition, these results confirm the previous research that the glass formation tendency decreases with increasing O/P ratio [25].

Physical Properties.

The density of a glass depends on molecular weight and packing volume. From Figure 3.3, we can conclude that density increases as the length of phosphate chains decreases. Compared with the CaO content, the Fe_2O_3 content will decrease the thermal expansion as shown in Figure 3.5. This is consistent with the previous research that found the addition of Fe_2O_3 leads to the formation of strong Fe-O-P bonds, which make the phosphate network much tighter and more cross-linked [4,15]. The iron additions can strengthen the cross-bonding between the polyphosphate chains and strengthen the bonding of the ends of these chains to the surrounding glass structure [5].

Figure 3.4 shows that iron oxide increases the Young's modulus of the Ca-Fe-phosphate glasses. This is similar to the effect on thermal expansion, in which iron additions strengthen the cross bonding between the phosphate chains and the ends of these chains to the surrounding glass structure.

CORROSION ANALYSIS

Bulk dissolution experiments reveal that the dissolution behavior of calcium iron phosphate glasses can be classified into three types, based on the weight loss and pH changes in LS solution (Figure 4.1).

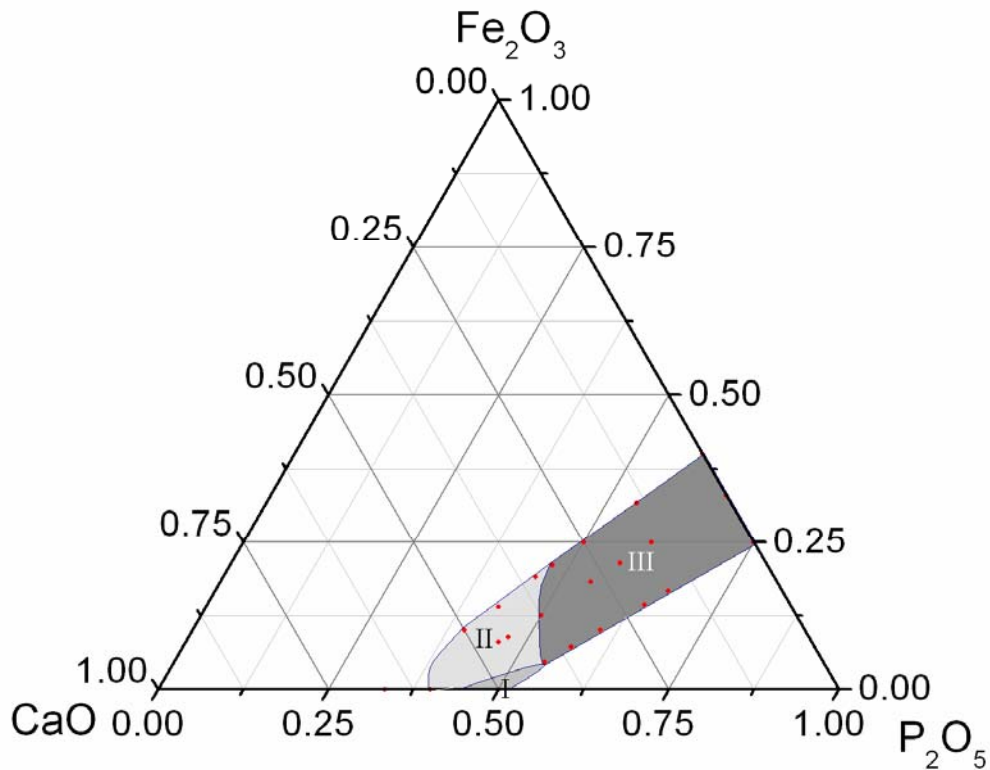


Figure 4.1. Classification of Ca-iron-phosphate corrosion behavior.

The type I behavior is represented by the glass CFP01. This calcium phosphate glass forms CaHPO_4 crystals after 500 hours and the pH of solution decreases to as low as 4. (In NaOH solutions, CFP01 powders formed $\text{Ca}_5(\text{PO}_4)_3\text{OH}$ crystals after 20 hours.)

Type II glasses include the CaO-rich poly- and pyrophosphate compositions. These are relatively stable compositions. The weight losses after 500 hours corrosion in LS are all less than $0.03\text{g}/\text{cm}^2$ and the pH of the LS does not change much (< 1.5 units) except for CFP21. CFP27 glass formed $\text{Ca}_5(\text{PO}_4)_3\text{OH}$ crystals, CFP21 and CFP52 grew more $\text{Ca}_2\text{P}_2\text{O}_7$ crystals.

The Fe_2O_3 -rich poly- and pyrophosphate glasses and Fe_2O_3 -containing metaphosphate glasses exhibit type III corrosion behaviors. The weight losses after 500 hours corrosion in LS are

between 0.06g/cm^2 to 0.09g/cm^2 and the solution pH dropped to ~ 7 . The corrosion species on the glass surfaces were either $\text{Ca}_5(\text{PO}_4)_3\text{OH}$ crystals or amorphous.

Figure 4.2 shows the calculated predominant calcium phases predicted to precipitate from solutions, using the equilibrium modeling software Predom2 and Medusa [26]. The aqueous environment was set to be similar to LS solution. The concentrations of other materials are based on weight loss calculations

. These predictions show that when pH drops below ~ 7 and PO_4^{3-} concentration is $> 0.05\text{mol/L}$, the stable precipitate is $\text{CaHPO}_4 \cdot 2\text{H}_2\text{O}$. When pH remains above 7, there is an area where the stable solid phase is $\text{Ca}_5(\text{PO}_4)_3\text{OH}$. $\text{Ca}_2\text{P}_2\text{O}_7$ will be stable at lower PO_4^{3-} concentrations and lower pH. The equilibrium phase modeling strongly supports the experimental results for the formation of $\text{Ca}_5(\text{PO}_4)_3\text{OH}$ crystals, as shown in Figure 3.13.

As shown in Figure 4.3 and Figure 4.4, the weight loss in Lawrence solution is strongly related to CaO and Fe_2O_3 concentration in the glass. Previous studies showed that the addition of both alkaline earth oxides, like CaO, and cross-linking agents, like Fe_2O_3 could effectively improve the glass durability [12,15-19,27-28]. The reason is that both modifiers can strengthen the cross-links between the phosphate chains. Figure 4.3 and Figure 4.4 indicate that CaO improves resistance to high pH solution corrosion more than Fe_2O_3 . Because the Ca-O-P bond is weaker than the Fe-O-P bond, they may be easier to hydrate. However, due to the low solubility of Ca-phosphate phases, protective coatings form on the glass surface, thereby limiting the rate at which further corrosion takes place. This may be the reason why calcium can improve glass durability.

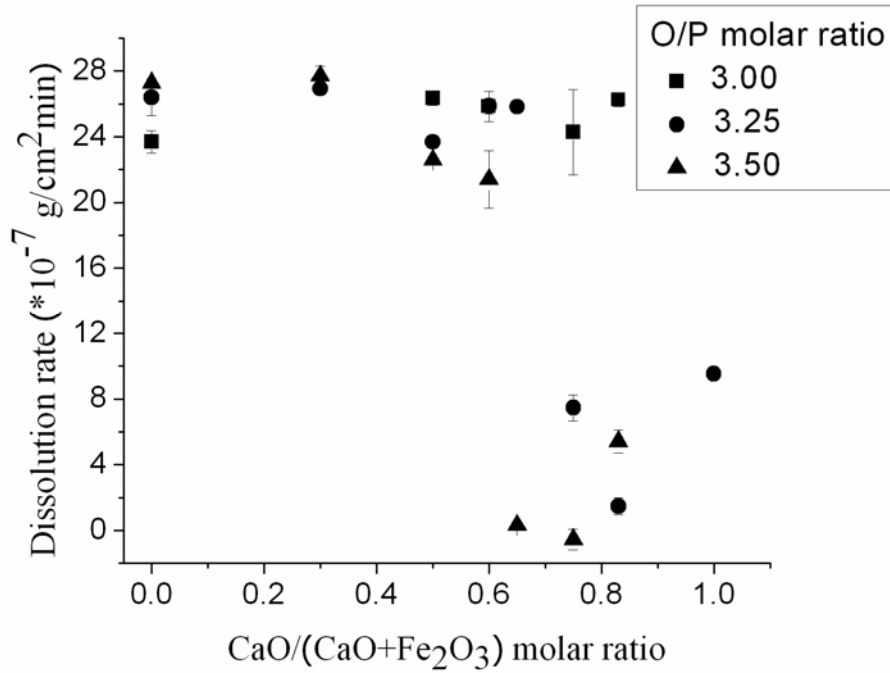


Figure 4.4. Dissolution rates of glasses immersed in LS for 500 hours at 80°C.

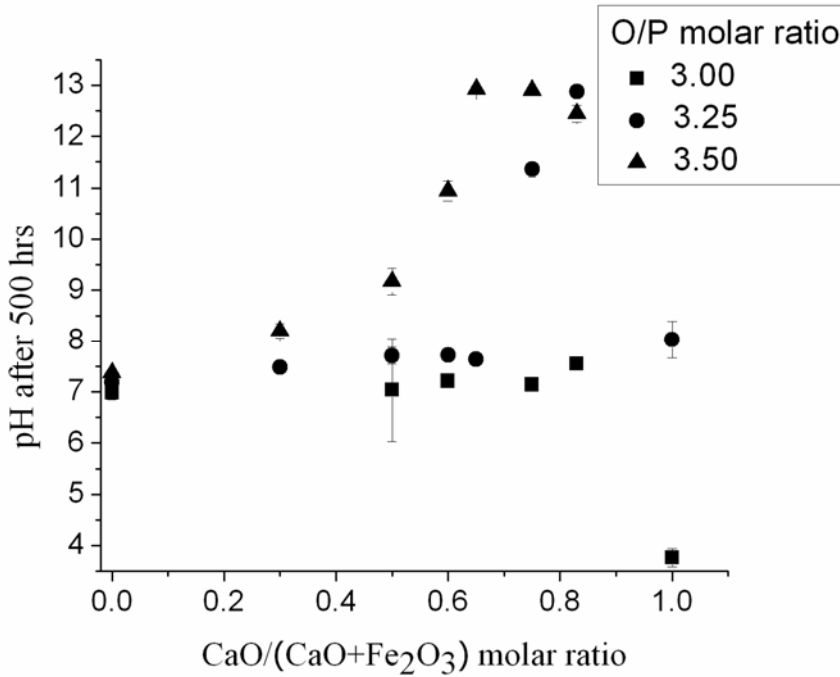


Figure 4.5. pH values of Lawrence solutions after 500 hours of glass corrosion at 80°C.

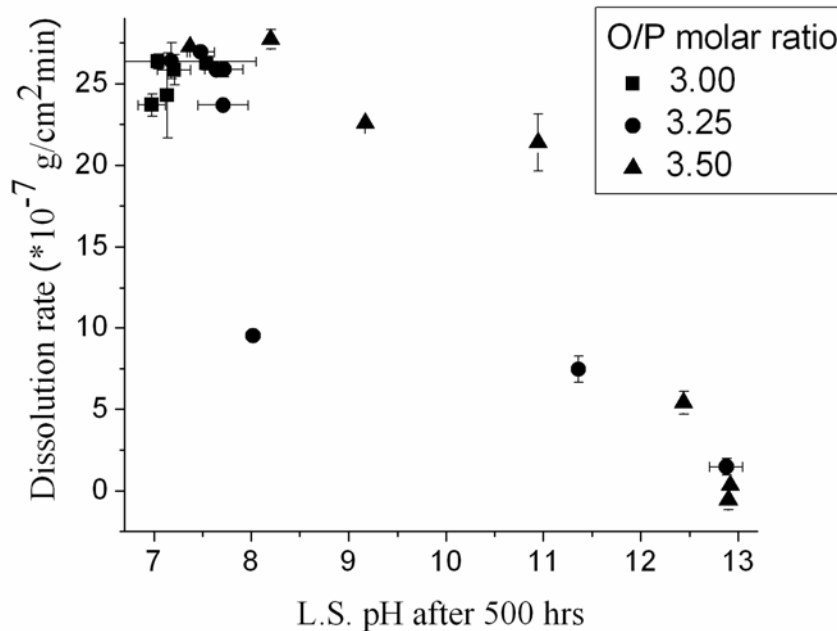


Figure 4.6. Dissolution rates of glasses vs. final pH of LS after 500 hours at 80°C.

The change in the pH of the Lawrence solution with corrosion time is another indication for the relative stability of the phosphate glasses to attack by alkaline solutions. Figure 4.5 summarizes the final pH of solutions after 500 hours of glass corrosion. In general, poly- and pyrophosphate glasses with high CaO-contents do not cause the significant drops (from the initial pH of 13) in solution pH as do glasses with low CaO-contents and/or metaphosphate structures. Figure 4.6 compares the corrosion rates with the final pH of the Lawrence solution. Those glasses with the greatest dissolution rates produce the lowest solution pH, a likely consequence of the formation of phosphoric acid in solution as the phosphate anions are released from the glasses.

CORROSION MECHANISM

For type I glass (CFP01), the dissolution rate is slow for the first 200 hours (Figure 3.6, 3.9 and 4.4). However, the dissolution rate increases and the pH value of the solution drops to acidic after 200 hours. The glass converts to CaHPO₄ crystals after 500 hours corrosion. The corrosion process depends on chain hydrolysis [12], where hydroxyl ions attacked the long phosphate chains, to release orthophosphate anions and form CaHPO₄ crystals. The H⁺ ions

released into the solution as a result of the chain hydrolysis causes the solution pH to drop. This reaction kept going on, therefore glass break up and solution pH decreased to acidic.

For type II □ glasses, XRD results showed that $\text{Ca}_5(\text{PO}_4)_3\text{OH}$ crystals form on corroded surfaces except for CFP04 which does not contain calcium oxide. For metaphosphate glasses (CFP02 and CFP03), the crystals loosely attached to the surface and hence are easily peeled off. But for pyrophosphate glass (CFP53), the crystals are still attached to the surface. Comparing Figure 3.15 and 3.17, the surface of CFP03 is much more fragile than that of CFP53, which confirms the previous conclusion. This also explains why metaphosphate glass immersed in LS solution kept on dropping pH until neutral, whereas pH of solution of CFP53 glass just dropped to about 9. The surface coating protection is more effective on pyrophosphate glasses than on metaphosphate glasses. Combining with XRD results that iron phosphate glasses formed Fe_2O_3 crystals after 20 hours corrosion in NaOH, it may be concluded that iron oxide releases from corroding glass react with hydroxyl ions and precipitated out the Fe_2O_3 crystals, while calcium oxide addition would form a protective Ca-phosphate coating on the glass surface.

For metaphosphate glasses, the dissolution behavior does not change significantly when the CaO and Fe_2O_3 concentrations change. Both Fe^{3+} and Ca^{2+} react with the OH^- , phosphate chain structure breaks up and releases different kinds of phosphate anions, resulting in the formation of $\text{Ca}_5(\text{PO}_4)_3\text{OH}$ and Fe_2O_3 . The reaction keeps going until the solution pH reaches ~7. Most of the reaction products are loosely attached to the glass surface, whether amorphous or crystalline. Afterwards, these products break up and new glass surface is exposed to alkaline attack.

For the pyrophosphate glass, when CaO concentration is high, well-adhered $\text{Ca}_5(\text{PO}_4)_3\text{OH}$ forms on the glass surface and very few PO_4^{3-} anions are released to the solution, indicating that a strong protective layer has formed to hinder further reaction. So iron oxides do not have much chance to participate in the reaction with alkaline solutions. EDS (Table 3.2) shows Ca/P increases after corrosion, while the Fe/P remained the same. When iron oxide concentration is high, Fe^{3+} will precipitate as Fe_2O_3 (results not shown here). This breaks the pyrophosphate structure, so the $\text{P}_2\text{O}_7^{4-}$ unit is released, ($\text{P}_2\text{O}_7^{4-} + \text{OH}^- \rightarrow 2\text{PO}_4^{3-} + \text{H}^+$), and

destroys the effect of iron on glass structure and makes the $\text{Ca}_5(\text{PO}_4)_3\text{OH}$ layer not so effective for protecting glass.

5. CONCLUSIONS

- 1) Compared with calcium oxide addition to the phosphate glasses, iron oxide addition can improve the glass and fiber forming ability, decrease thermal expansion and increase Young's modulus. This is because of the cross-link effect of iron oxide.
- 2) Dissolution rate in alkaline solution decreases with phosphate chain length.
- 3) Calcium oxide addition can improve glass durability in pyrophosphate glasses, the glass structure remains after corrosion, low concentration of phosphate anions are released to the solution. This is because calcium can form a protective layer on the glass surface which hinders the further reaction.
- 4) The improvement of calcium oxide is not as remarkable in metaphosphate glasses as pyrophosphates. Most metaphosphate glasses hydrolyze in high pH solution, forming orthophosphate anions and releasing H^+ ions, which decrease the solution pH.

BIBLIOGRAPHY

- [1] A. J. Majumdar, and R. W. Nurse, "Invited review: glass fiber reinforced cement," *Mater. Sci. Engng*, **15** 107-127 (1974).
- [2] L. J. Larner, K. Speakman, and A. J. Majumdar, "Chemical interactions between glass fibers and cement," *Journal of Non-Crystalline Solids*, **20(1)** 43-74 1976.
- [3] S. T. Reis, M. Karabulut, and D. E. Day, "Chemical durability and structure of zinc-iron phosphate glasses," *Journal of Non-Crystalline Solids*, **292(1-3)** 150-157 (2001).
- [4] B. Kumar and S. Lin, "Redox state of iron and its related effects in the $\text{CaO-P}_2\text{O}_5\text{-Fe}_2\text{O}_3$ glasses," *J. Am. Ceram. Soc.*, **74(1)** 226-28 (1991).
- [5] B. C. Sales, and L. A. Boatner, "Physical and chemical characteristics of lead-iron phosphate nuclear waste glasses," *Journal of Non-Crystalline Solids*, **79(1-2)** 83-116 (1986).
- [6] T. R. Gentry, "Life assessment of glass fiber reinforced composites in Portland cement concrete," *Proceedings of the American Society for Composites, Technical Conference*, **16** 446-457 (2001).
- [7] S. Diamond, "Effects of two Danish flyashes on alkali contents of pore solutions cement flyash pastes," *Cement and Concrete Research*, **11** 383-394 (1981).
- [8] V. T. Yilmaz and F. P. Glasser, "Reaction of alkali-resistant glass fibers with cement, part 1," *Glass Technology*, **32** 91-98 (1991).

- [9] S. M. Budd, "The mechanisms of chemical reaction between silicate glass and attacking agents," *Physics and Chemistry of Glasses*, **2** 111-114 (1961).
- [10] G. Scarinci, D. Soraru, G. Grassi, G. Stafferri and C. Badini, "Portland cement reinforced with new alkali resistant glass fibres," *Proc. 8th Int. Congr on the Chem of Cement*, **6** 381-383 (1986).
- [11] V. T. Yilmaz, "Chemical attack on alkali-resistant glass fibers in a hydrating cement matrix," *J. Non-Cryst. Solids*, **151** 236-244 (1992).
- [12] B. C. Bunker, G. W. Arnold and J. A. Wilder, "Phosphate glass dissolution in aqueous solutions," *J. Non-Cryst. Solids*, **64** 291-316 (1984).
- [13] B.S. Bae and M.C. Weinberg, "Chemical durability of copper phosphate glasses," *Glass Technology*, **35** 83-88 (1994).
- [14] D. Cacaina and S. Simon, "calcium influence on dissolution rates of potassium phosphate glasses," *Journal of Optoelectronics and Advanced Materials*, **5** 191-194 (2003).
- [15] X. Yu, D. E. Day, G. J. Long, and R. K. Brow, "Properties and structure of sodium iron phosphate glasses," *J. Non-Cryst. Solids*, **215** 21-31 (1997).
- [16] X. Feng, and T. B. Metzger, "A glass durability model based on understanding glass chemistry and structural configurations of the glass constituents," *Materials Research Society Symposium Proceedings*, **432** 27-38 (1997).
- [17] J. Clement, G. Avila, M. Navarro, S. Martinez, M.P. Ginebra and J.A. Planell, "Chemical durability and mechanical properties of calcium phosphate glasses with addition of Fe₂O₃, TiO₂ and ZnO," *Key Engineering Materials*, **192-195** 621-624 (2001).
- [18] Y.M. Moustafa, "Characterization of iron oxychloride potassium phosphate glasses," *J. Phys. D*, **32** 2278-2286 (1999).
- [19] G.N. Greaves, S.J. Gurman, L.F. Gladden, B. C. Sales and R.N. Jenkins, "A structural basis for the corrosion resistance of lead iron phosphate glasses," *Philosophical Magazine B*, **58** 271-283 (1988).
- [20] I.W. Donald, B.L. Metcalfe, S.K. Fong and L.A. Gerrard, "The influence of Fe₂O₃ and B₂O₃ additions on the thermal properties, crystallization kinetics and durability of a sodium aluminum phosphate glass," *J. Non-Cryst. Solids*, **352** 2993-3001 (2006).
- [21] Ohtomo, Koichiro, Yoshimura, and Takuji, "Alkali resistant glass compositions and alkali resistant glass fibers prepared therefrom," U.S. Pat. No. 3,973,974 (1976).
- [22] R.K. Brow, D.R. Tallant, S.V. Crowder, S.K. Saha, H. Jain, A. McIntyre and D. E. Day, "Advanced materials for aerospace and biomedical applications," Sandia Report 96-2772, (1996).
- [23] B. C. Sales, L. A. Boatner and J. O. Ramey, "Intermediate range order in simple metal phosphate glasses," *J. Non-Cryst. Solids*, **232-234** 107-112 (1998).
- [24] T. R. Meadowcroft and F. D. Richardson, "Structural and thermodynamic aspects of phosphate glasses," *Trans. Faraday Soc*, **61** 54-70 (1965).
- [25] D. E. Day, Z. Wu, C. S. Ray and P. Hrma, "Chemically durable iron phosphate glass waste forms," *J. Non-Cryst. Solids*, **241** 1-12 (1998).
- [26] <http://www.kemi.kth.se/medusa/> Medusa and Predom2 software, July 2007.
- [27] R. K. Brow, "Review: the structure of simple phosphate glasses," *J. Non-Cryst. Solids*, **263** 1-28 (2000).
- [28] B. C. Sales, L. A. Boatner and J. O. Ramey, "Chromatographic studies of the structure of amorphous phosphates," *J. Non-Cryst. Solids*, **263-264** 155-166 (2000).

Section 2

Flexural Tests of Fiber-Reinforced Cement Composites

Rossella Mafalda Ferraro¹ and Richard K. Brow²

¹Civil and Architectural Engineering

²Materials Science & Engineering Department

ABSTRACT

Glass fiber-reinforced cement (GRFC) composites were fabricated using corrosion-resistant glass fibers developed at UMR in collaboration with Mo-Sci, Inc. (Rolla, MO). The flexural strengths of the composites were evaluated using three-point flexural tests, and these strengths were compared with those of composites formed with commercial silicate glass fibers. Composites produced with uncoated UMR phosphate glass fibers had flexural strengths that, after seven days of curing, exceeded by about 30% the flexural strengths of fiber-free cement coupons, comparable to the strengths of composites made with uncoated silicate fibers, but about 50% lower than the strengths of composites made with commercially-coated alkaline resistant glass fibers. After 28 days, the mechanical advantage of fiber reinforcement with coated and uncoated phosphate and silicate fibers was lost. Evidence for corrosion of the fiber surfaces was found in post-mortem analyses of the test coupon, and this evidence was consistent with the corrosion models described in the first section of this report.

1. INTRODUCTION

FLEXURAL TESTING

The flexural test method—also known as a transverse beam test—measures the behavior of materials subjected to simple beam loading. Flexural properties are an essential factor in the determination of stiffness from a compression or tensile loadings. In bending, a beam is subjected to both compression and tensile stresses.

With this test, maximum composite stress and maximum strain are calculated for different increments of load, and in the end, all results are plotted in a stress-strain diagram. Flexural strength is the maximum stress calculated at the surface of the specimen on the convex or tension side. Flexural modulus is calculated from the slope of the stress vs. deflection curve; if the curve has no linear region, a secant line is fitted on the curve to determine the slope.

A flexure test produces tensile stress in the convex side of the specimen and compression stress in the concave side. This combination then creates an area of shear stress along the midline. To ensure the primary failure comes from tensile or compression stress, the shear stress must be minimized. This is done by controlling the span-to-depth ratio (the length of the outer span divided by the height of the specimen). For most materials, $S/d=16$ is acceptable, but some materials require $S/d=32$ to 64 to keep the shear stress low enough.

Flexural testing is often done on relatively flexible materials such as polymers, wood, and composites; accordingly, two test procedures are typically used:

- 3-point flex
- 4-point flex

In a 3-point test, the area of uniform stress is quite small and concentrated under the center loading point; whereas, in a 4-point test, the area of uniform stress exists between the inner span loading points (typically half the outer span length).

The 3-point bending flexural test provides values for the modulus of elasticity in bending (E_B), flexural stress (σ_f), flexural strain (ϵ_f), and the flexural stress-strain response of the material. The main advantage of a 3-point flexural test is the ease of the specimen preparation and testing. However, this method has also some disadvantages. In particular, the results of the testing method are sensitive to specimen and loading geometry and strain rate.

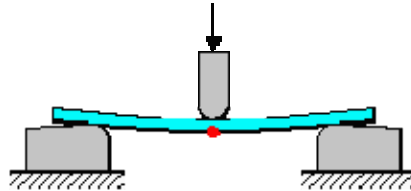


Figure 1: Flexural test configuration and location of the maximum stress/strain

The 3-point flexural test is the most common for polymers, and specimen deflection is usually measured by the crosshead position. The 4-point flexural test is common for wood and composites; in this case, the test requires an electrometer to accurately measure specimen deflection at the center of the support span. When a 3-point flexural test is done on a brittle material like ceramic or concrete, it is often called the Modulus of Rupture (MOR). This test provides flexure strength data only, not stiffness (modulus).

FLEXURAL TESTS ON GFRC

Flexural strength is one measure of strength of concrete and is expressed as the Modulus of Rupture (MOR) in MPa (psi); in addition, it is determined using standard test methods—ASTM 78 (third-point loading) or ASTM C 293 (center-point loading).

Flexural MOR is about 10 to 20 percent of compressive strength depending on type, size, and volume of the coarse aggregate used. However, the best correlation for specific materials is obtained by laboratory tests for given materials and mix design. The MOR determined by center-point loading is lower than the MOR determined by third-point loading, sometimes by as much as 15 percent.

Using a flexural test for cementitious material is a very common practice for designers of pavement materials. Therefore, laboratory mix design based on a flexural strength test may be required, or cementitious material data may be selected from past experience to obtain the needed design MOR. Some also use MOR for field control and acceptance guidelines for pavements; very few use flexural testing for structural concrete. Agencies not using flexural strength for field control generally find the use of compressive strength convenient and reliable to judge the quality of the concrete as delivered.

In our case, we tested the concrete reinforced by different kinds of fibers with both tests, flexural and compression, trying to avoid every possible error and to understand the mechanical behavior as much as possible.

2. Experimental Procedures

Corrosion-resistant iron phosphate glass (SIP) fibers were manufactured at Mo-Sci and used to prepare glass fiber-reinforced cement (GFRC) composite samples. Table 1 indicates the nominal compositions of these glasses. The SIP fibers were 15-25 microns in diameter, and were pulled from platinum bushings at Mo-Sci. In addition, commercially available silicate glass fibers were also tested, including the alkaline-resistant 'Cem-FIL' composition and a conventional 'E-glass' composition. One set of Cem-FIL fibers were used with their original polymer coatings (Cem-FIL-c) to make GFRCs and one set of fibers were used to make GFRCs after that coating was removed by pyrolyzing in air at 600°C overnight. The E-glass fibers retained their originally manufactured coatings (E-glass-c). No coatings were used for the SIP reinforcing fibers.

Table 1. Nominal chemical compositions of selected iron phosphate glasses

mol%	SIP-91	SIP-115	SIP-121
P ₂ O ₅	48	48	48
CaO	18	20	20
NiO	4	0	0
MgO	6	15	12
SiO ₂	5	3	3
Fe ₂ O ₃	0	4	0
Y ₂ O ₃	4	2.4	4
TiO ₂	4	0	6
MnO ₂	0	0.6	0
CaF ₂	8	0	0
BaO	3	7	7

GFRC test coupons were sectioned from larger panels that were cast into molds using the following compositions:

- a) 3942.43g of Cement Portland
- b) 2628.29g of sand
- c) 1423.66g of water
- d) 187.01g of fiber

The preparation starts with mixing the cement paste and the sand, without water, for 1±0.3 minutes. After this time, 75 percent of total water is added, and everything is mixed for other 1±0.3 minutes. Next, the remaining 25 percent of total water is added, and all are mixed for an additional minute. Glass fibers with chopped lengths of ~ 15 mm are then added to the mixture by hand. The composite mixture is added to the panel mold, which is set on a vibration table, where the mixture is homogenized and the air bubbles are removed. After the vibration, the mixture in the mold is cured for 24 hours in a plastic bag and the resulting panel is then cut into 12 bars (225.6x50.8x12mm) for MOR testing. The bars are then further cured in water at 73±5°F either for seven days or for 28 days, before they are tested.

All GFRCs were tested using the procedures outlined in ASTM C 947 – 03, Standard Test Method for Flexural Properties of Thin-Section Glass-Fiber-Reinforced Concrete (Using Simple Beam with Central-Point Loading). The following equations were used to calculate the composite properties:

- Flexural yield strength:

$$F_y = \frac{P_y L}{bd^2} \quad (1)$$

- Flexural ultimate strength:

$$F_u = \frac{P_u L}{bd^2} \quad (2)$$

- Modulus of Elasticity:

$$E = \frac{23P_y L^3}{108Y_y bd^3} \quad (3)$$

b = width of specimen

d = depth of specimen

P_y = force at the point on the force-deflection curve where the curve deviates from linearity

P_u = maximum force achieved by the specimen

F_y = flexural yield strength

F_u = flexural ultimate strength

L = major support span

E = Modulus of Elasticity

The following is a brief summary of the experimental procedures:

- **Samples**

- 1 panel each for 7 and 28 day curing
- 1 panel per fiber loading; fiber length 15 mm cut by hand using paper cutter
- 2.22 percent by volume fiber loading added to no fiber composition
- No fiber composition
 - Water:Cement = 1:3 fixed by weight
 - Sand:Cement = 2:3 fixed by weight

- **Sample preparation**

- Dry mix 1±0.3 minutes
 - 48.5 percent by weight cement paste
 - 32.3 percent by weight sand
- Add 75 percent of total water
- Mix 1±0.3 min.
- Add 25 percent of total water
- Mix 1±0.3 min.
- Add fiber by hand
- Mix 3±0.15 min.
- Cast

- Vibrate 5 minutes
- Cure 24 hours in plastic bag
- De-mold
- Cut 6 of 228.6 x 50.8 x 12 mm bars for MOR
- Save remnants for microscopy
- Cure in 73±5F water for 7 days
- Remove sample from water and test immediately after 7 days curing
- Spray with water during testing to eliminate evaporation
- Number and label samples
- Measure samples
- **Testing**
 - Six specimens were tested after 7 days curing in water, and 6 were tested after 28 days
 - The tests were conducted using the INSTRON test machine in McNutt Hall at UMR
 - Crosshead speed was set at 0.02 mm/min
 - The major support span, L, for the flexural test is 202 mm

3. Results and Discussion

FLEXURAL TESTS

Figures 2-8 show the stress-strain curves collected from the GFRC samples after seven days of curing, and figures 9-15 show the stress-strain curves collected from samples after 28 days of curing. Table 2 summarizes the strength calculations based on these results. The respective individual data sets are given in the Appendix to this report.

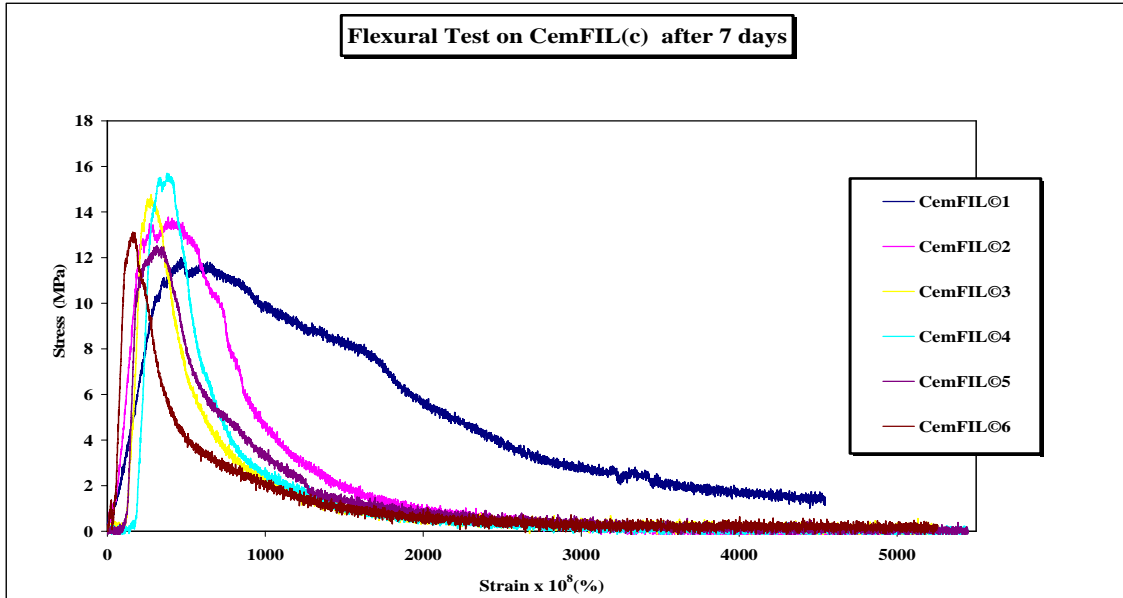


Figure 2: Stress-strain responses of GFRCs with coated CemFIL fibers, tested after 7 days.

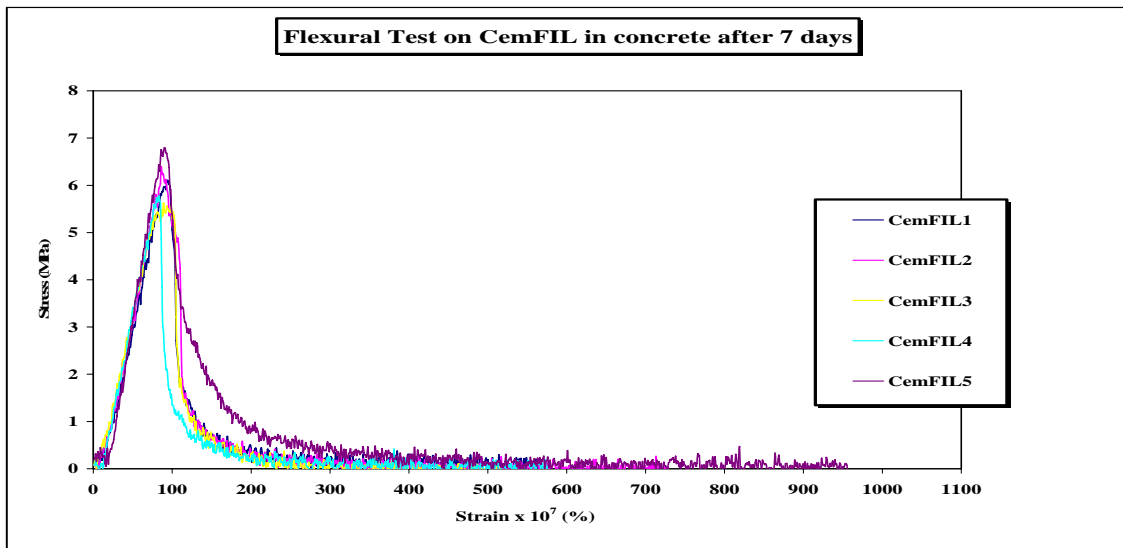


Figure 3: Stress-strain responses of GFRCs with uncoated CemFIL fibers, tested after 7 days.

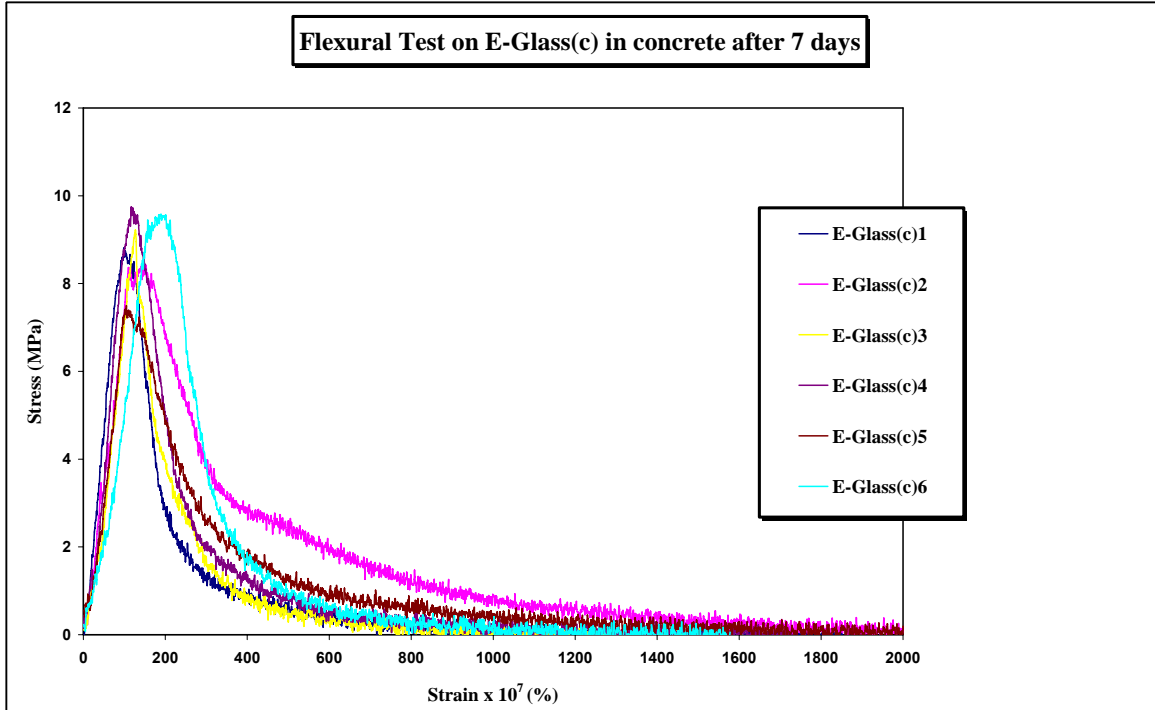


Figure 4: Stress-strain responses of GFRCs with coated E-glass fibers, tested after 7 days.

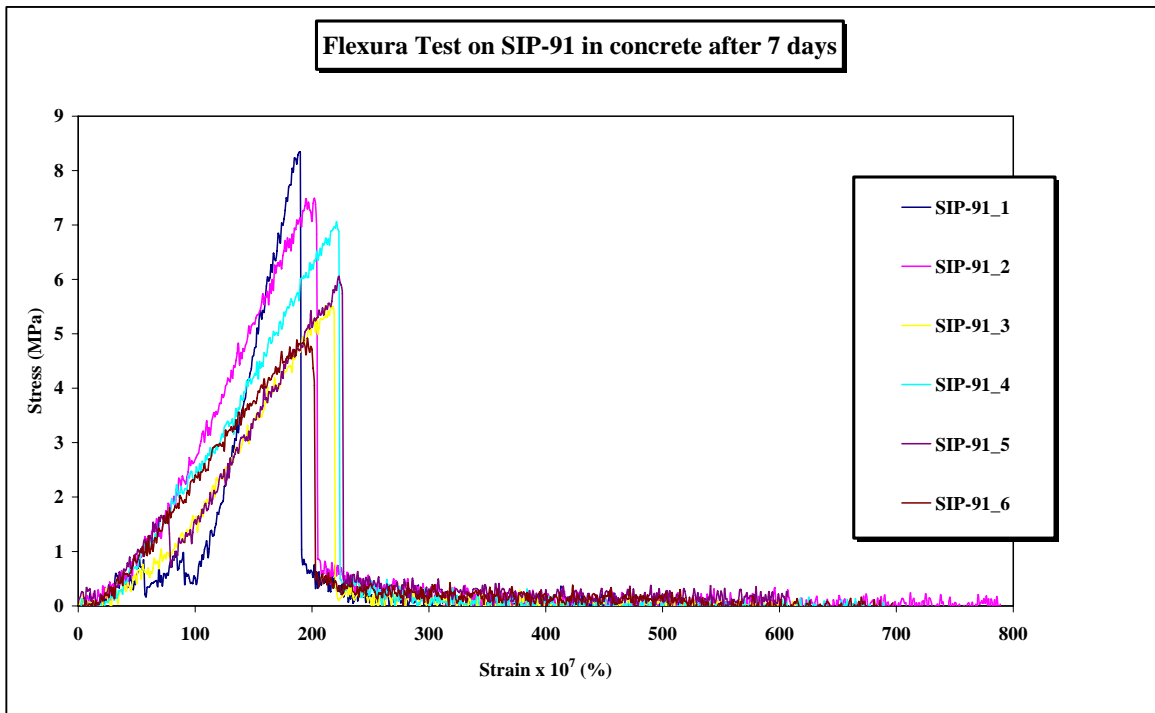


Figure 5: Stress-strain responses of GFRCs with uncoated SIP-91 fibers, tested after 7 days.

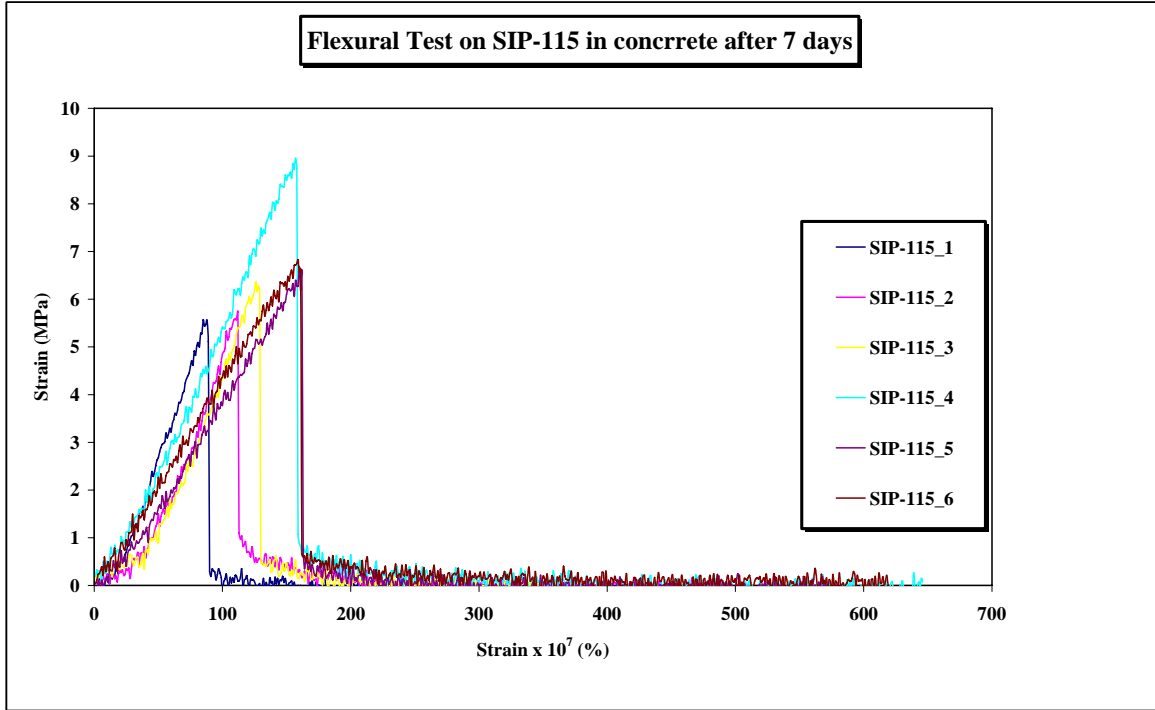


Figure 6: Stress-strain responses of GFRCS with uncoated SIP-115 fibers, tested after 7 days.

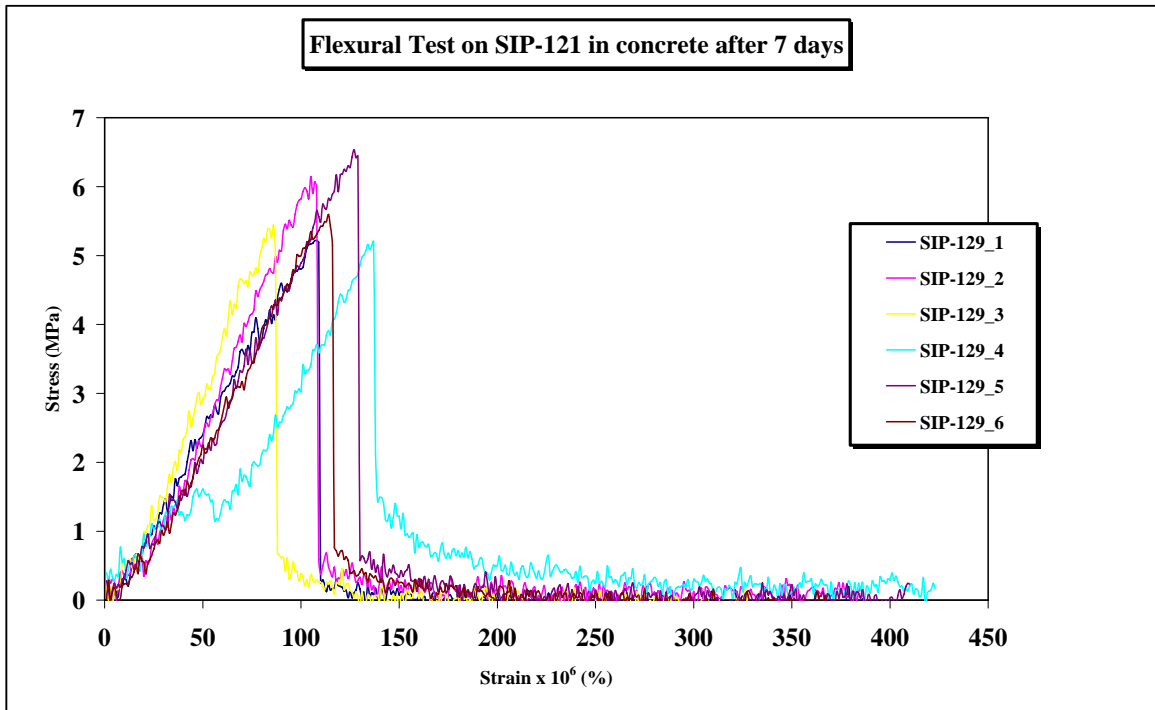


Figure 7: Stress-strain responses of GFRCS with uncoated SIP-121 fibers, tested after 7 days.

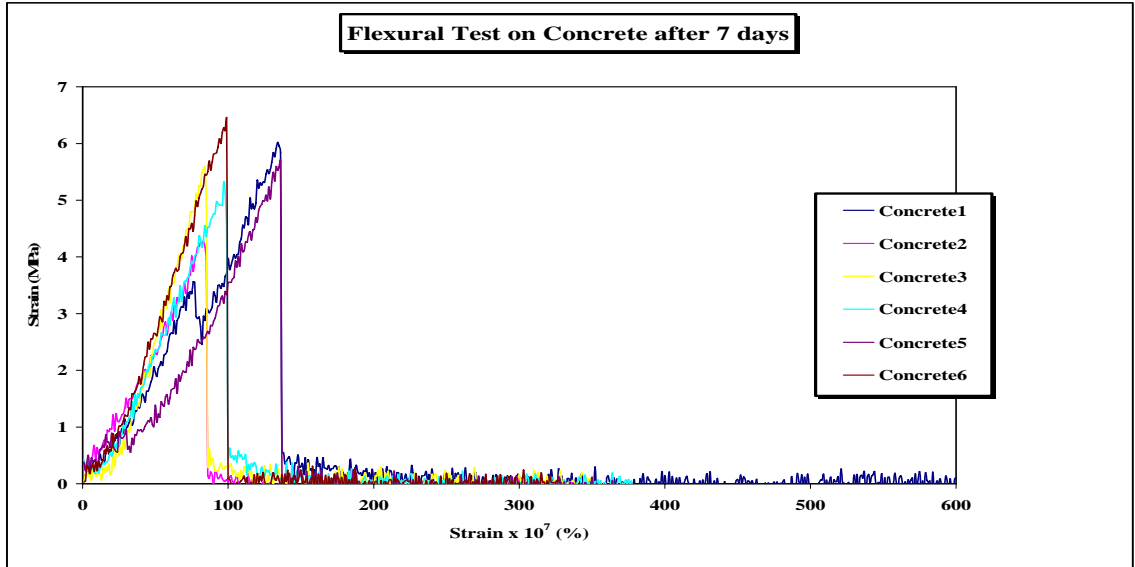


Figure 8: Stress-strain responses of neat cement, tested after 7 days.

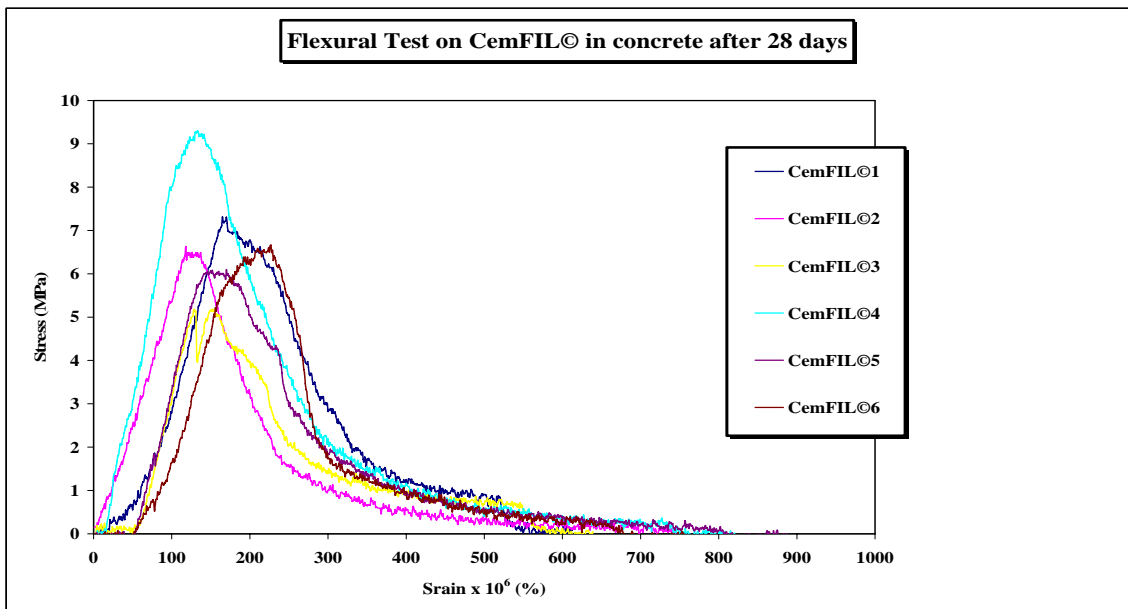


Figure 9: Stress-strain responses of GFRCs with coated CemFIL fibers, tested after 28 days.

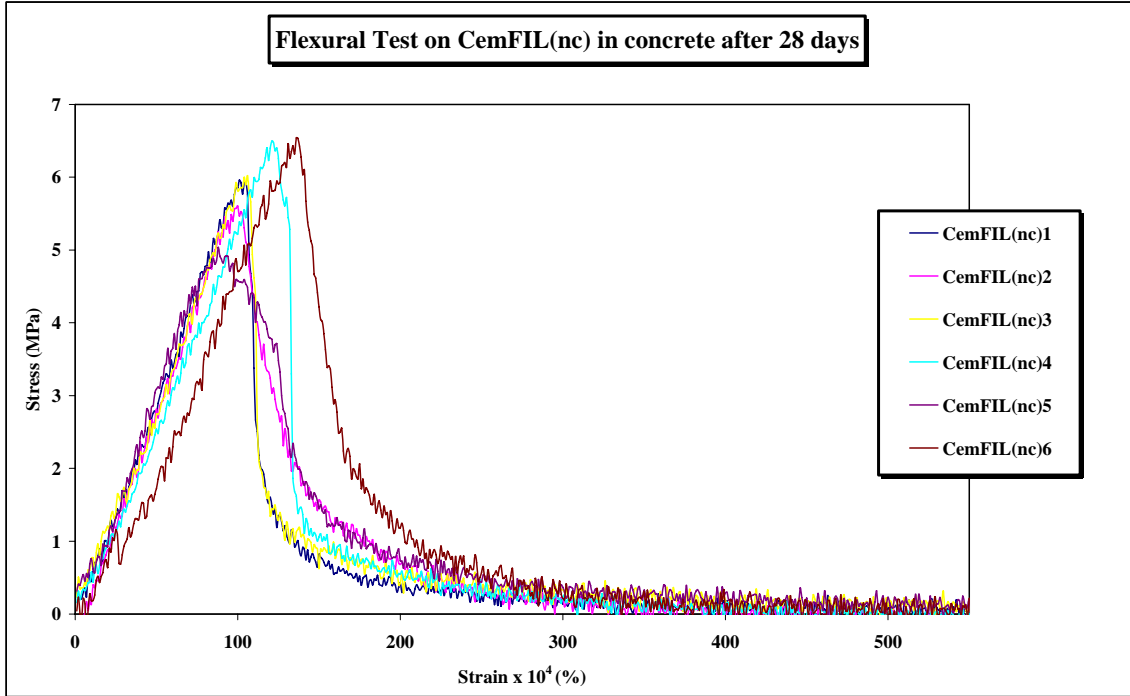


Figure 10: Stress-strain responses of GFRCs with uncoated CemFIL fibers, tested after 28 days.

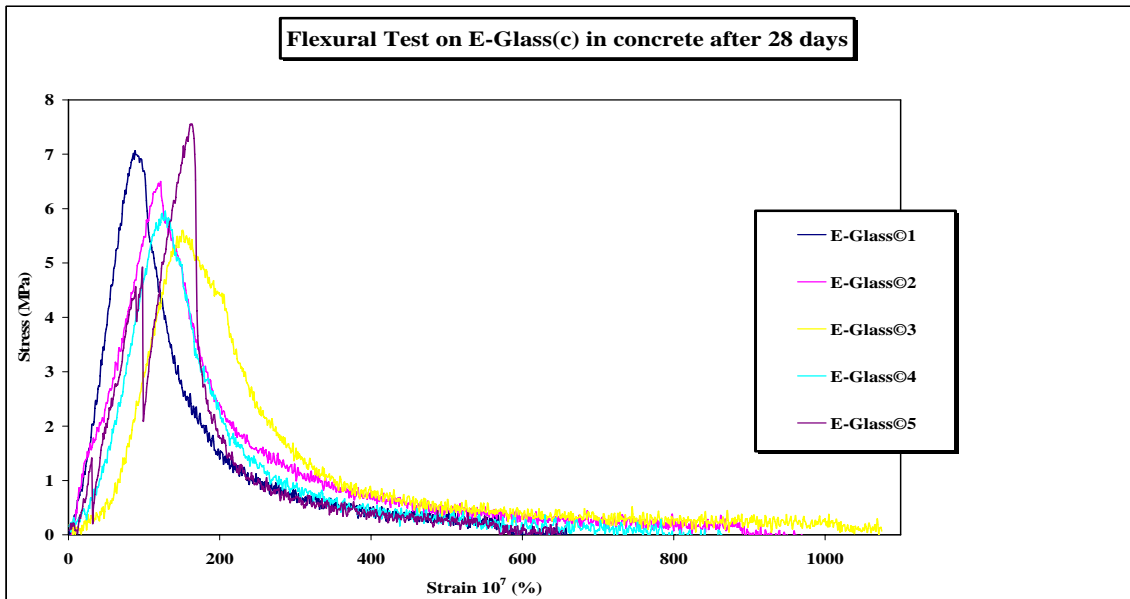


Figure 11: Stress-strain responses of GFRCs with coated E-glass fibers, tested after 28 days.

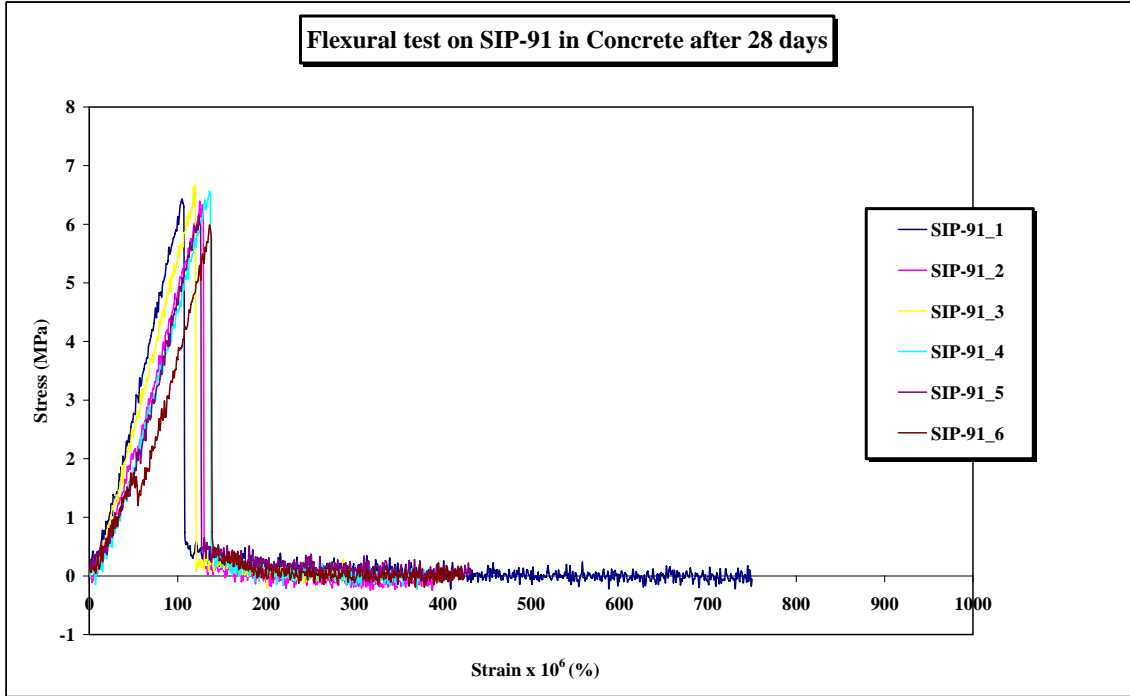


Figure 12: Stress-strain responses of GFRCs with uncoated SIP-91 fibers, tested after 28 days.

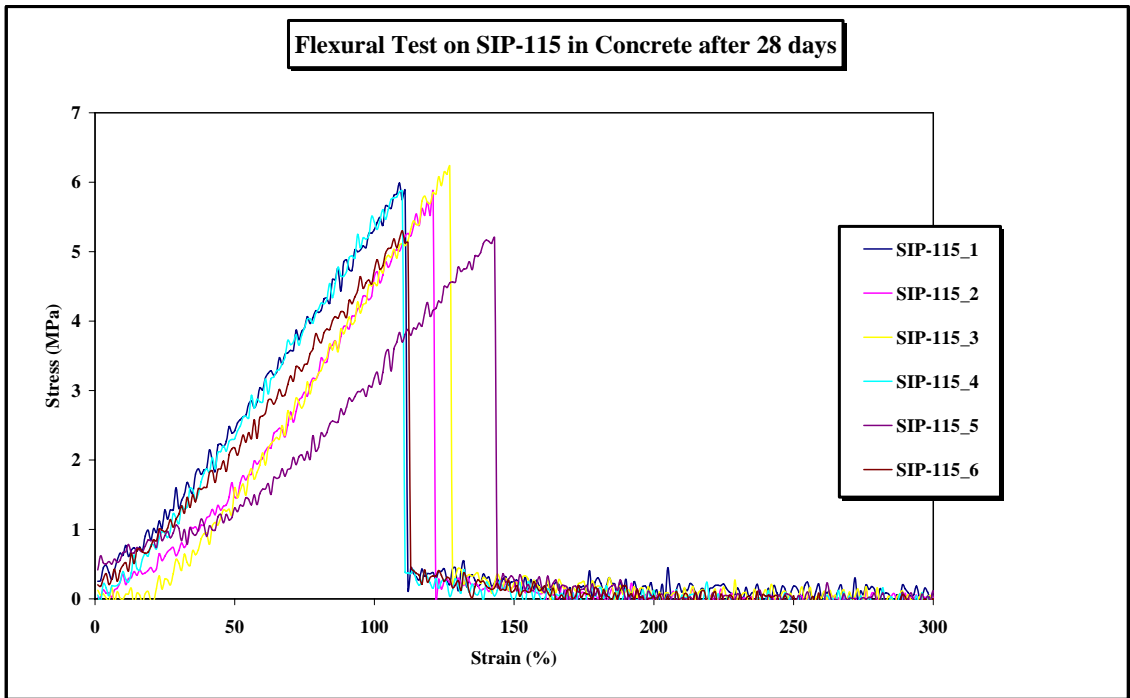


Figure 13: Stress-strain responses of GFRCs with uncoated SIP-115 fibers, tested after 28 days.

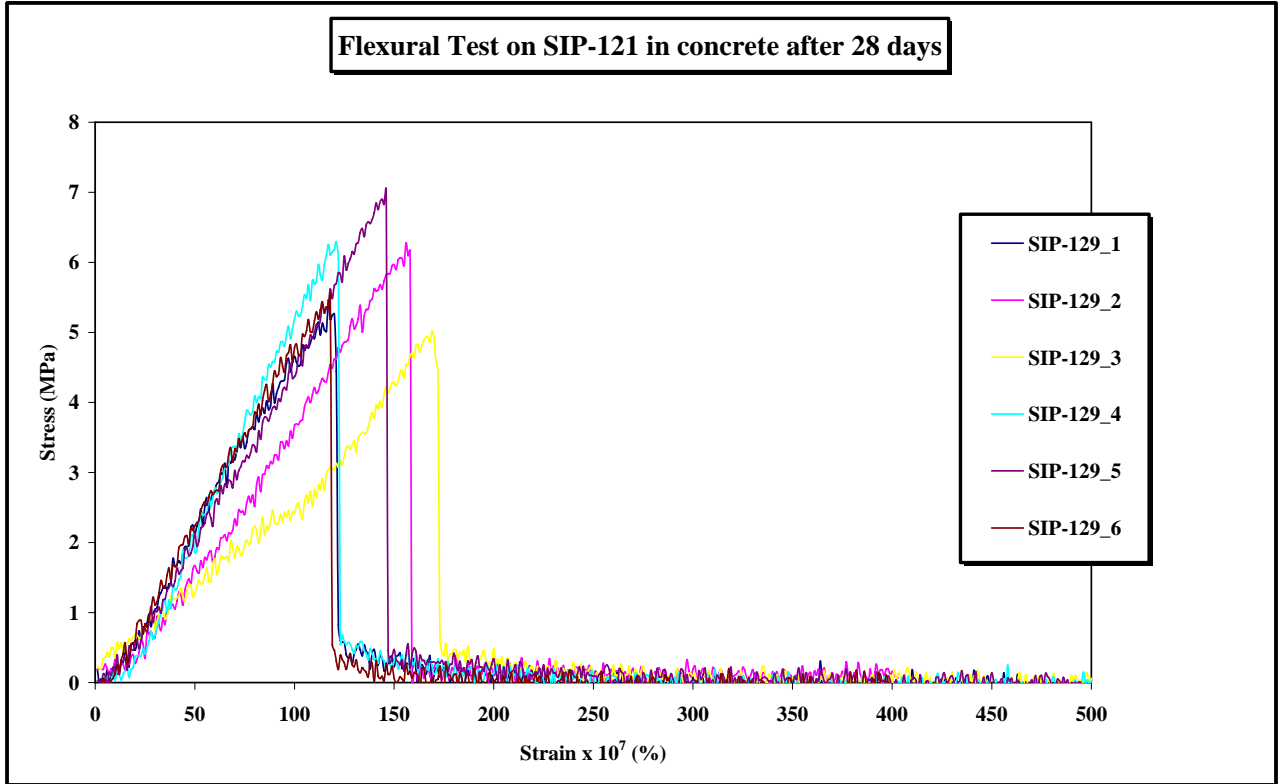


Figure 14: Stress-strain responses of GFRCs with uncoated SIP-121 fibers, tested after 28 days.

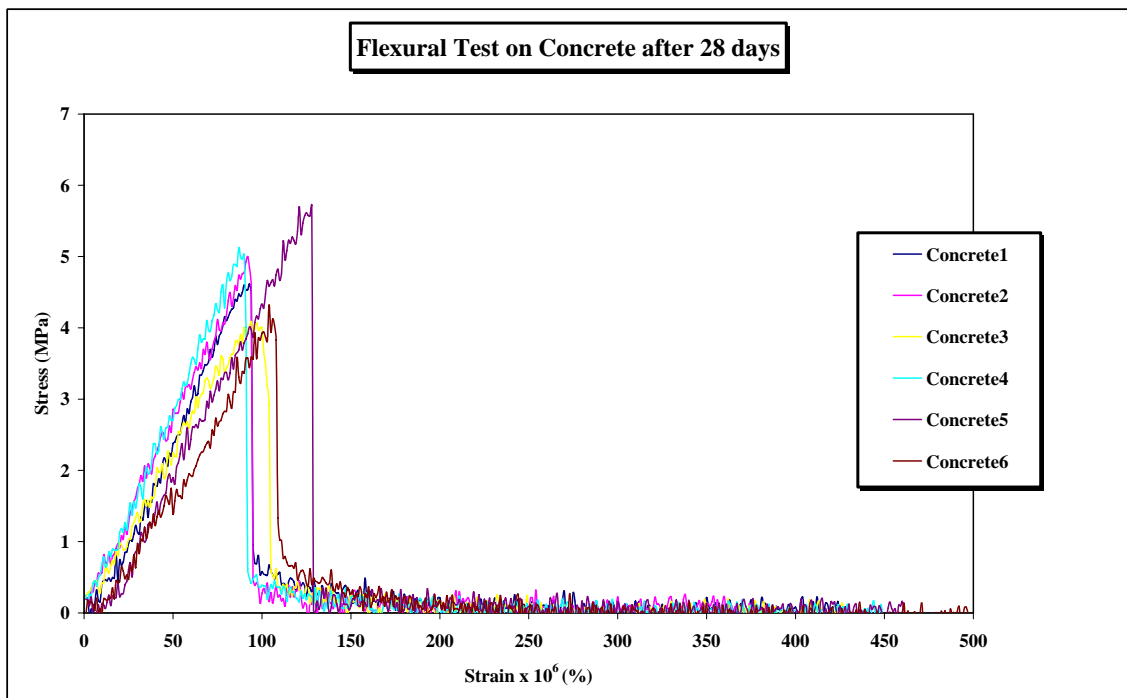


Figure 15: Stress-strain responses of neat cement, tested after 28 days.

Table 2: Summary of the flexural tests of the GFRCs.

Type of glass fiber	Average flexural yield strength (MPa) at 7 days	Average flexural yield strength (MPa) at 28 days	Average flexural ultimate strength (MPa) at 7 days	Average flexural ultimate strength (MPa) at 28 days	Average Modulus of Elasticity (MPa) at 7 days	Average Modulus of Elasticity (MPa) at 28 days
CemFIL-c	9.65	5.40	13.64	6.86	703	517
CemFIL	5.71	4.99	6.14	5.94	620	604
E-Glass-c	6.57	5.03	8.88	6.54	657	541
SIP-91	5.75	5.48	6.56	6.36	632	644
SIP-115	5.68	4.79	6.69	5.79	674	631
SIP-121	4.69	4.86	5.69	5.94	636	645
Concrete	4.07	4.96	4.81	5.56	661	656

MICROSCOPIC ANALYSES

Optical micrographs of the fracture surfaces of several GFRC coupons are shown in figures 16-21. In general, the coated fibers show less obvious reaction products on their surfaces, and exhibit greater fiber 'pull-out' behavior, than the coated fibers, consistent with the respective flexural test results. More detailed analyses are included in Section 3 of this report.

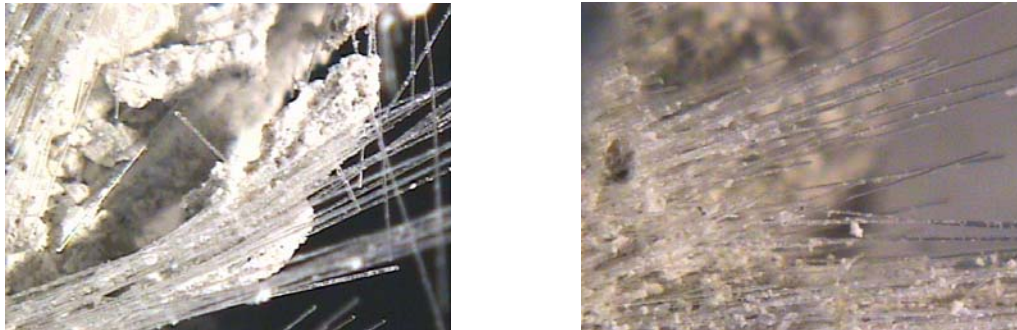


Figure 16: Optical micrographs of the fracture surfaces of GFRC coupons made with coated CemFIL fibers after curing for 7 days (left) and 28 days (right).

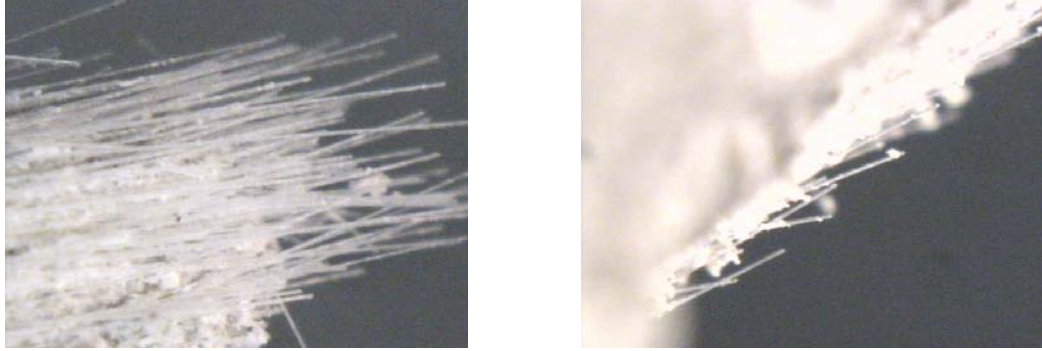


Figure 17: Optical micrographs of the fracture surfaces of GFRC coupons made with uncoated CemFIL fibers after curing for 7 days (left) and 28 days (right).

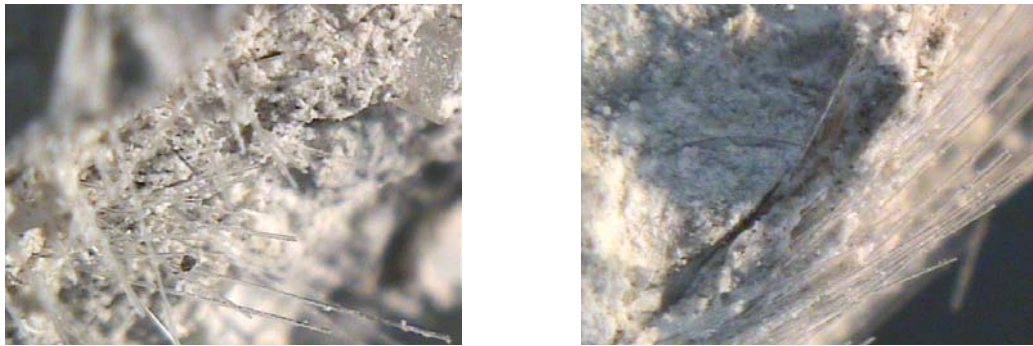


Figure 18: Optical micrographs of the fracture surfaces of GFRC coupons made with coated E-glass fibers after curing for 7 days (left) and 28 days (right).



Figure 19: Optical micrographs of the fracture surfaces of GFRC coupons made with uncoated SIP-91 glass fibers after curing for 7 days (left) and 28 days (right).

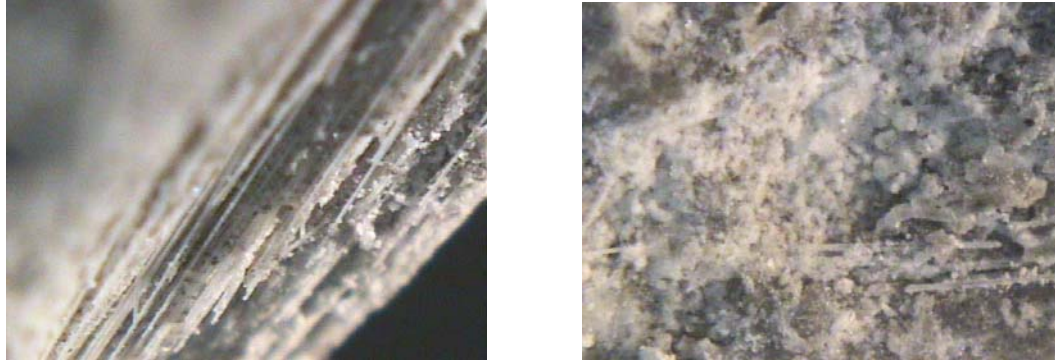


Figure 20: Optical micrographs of the fracture surfaces of GFRC coupons made with uncoated SIP-115 glass fibers after curing for 7 days (left) and 28 days (right).

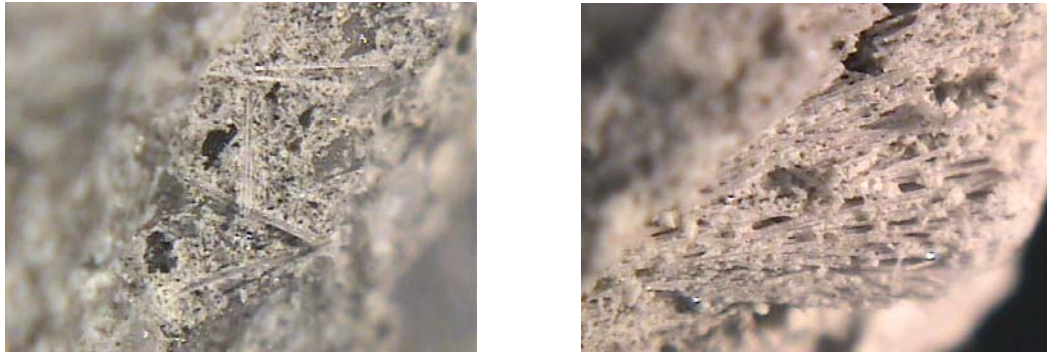


Figure 21: Optical micrographs of the fracture surfaces of GFRC coupons made with uncoated SIP-121 glass fibers after curing for 7 days (left) and 28 days (right).

Table 2 compares the properties of the different kinds of GFRCs tested. Several trends can be noted. For example, the flexural yield (F_y) and ultimate (F_u) strengths for the GFRCs decrease between 7 and 28 days of curing, whereas the neat cement coupon strengths increase. The coupons with the coated E-Glass fibers showed the largest decline. The greatest flexural strengths were found for the coated CemFIL coupons. The uncoated fibers, both CemFIL and SIP, imparted about the same increase in strength for GRFC coupons after seven days of curing, compared with the neat cement coupons, but that advantage is lost after 28 days of curing when the GRFC coupons made with uncoated fibers have about the same strength as the coupons made with neat cement. The different fibers have little effect on the modulus of elasticity for the GRFCs. The modulus of elasticity is the mathematical description of the tendency of an object to be deformed when a force is applied to it, and it is given from the stress-strain ratio (in this case, from Equation 3). This equation is used if a deflection is applied at the center of the major span to measure specimen deflection for the purpose of minimizing the effect of machine and fixture stiffness. The coated coupons made with coated CemFIL fibers, and to a lesser extent, coated E-

glass fibers, do exhibit a greater degree of toughness than the coupons made with uncoated fibers or neat cement. This toughness is likely associated with the enhanced 'pull-out' behavior of the coated fibers, as indicated in the respective optical micrographs shown above.

4. Conclusions

The initial (seven-day) flexural strengths of the glass fiber reinforced cement composite coupons exceed the flexural strengths of the neat cement coupons, and the coated fibers impart the greatest strengths of all samples tested. Comparing the stress-strain curves of the coated and uncoated CemFIL fiber GFRC's (figures 2 and 3, respectively) reveals the mechanical advantage that is at least temporarily imparted by the coated fibers. The large strain before total failure associated with the coated fiber composites indicate that these materials are tougher than those prepared from uncoated fibers, which exhibit a much more brittle failure behavior.

The uncoated phosphate fibers provide a temporary mechanical advantage for GRFC's compared to neat cement samples. After seven days of curing, the uncoated phosphate fiber samples have flexural strengths that are about 30% greater than that of the neat cement coupons. However, the flexural yield strengths of the uncoated and uncoated fiber-reinforced composites, both phosphate and silicate, decrease with time until after 28 days, there is no substantial difference between their strengths and those of the neat cement coupons.

Appendix 1- Flexural Test Results

Table A-1: Sample dimensions and stress-strain responses of GFRC coupons with coated CemFil fibers, tested after 7 days.

Sample	b,mm	d,mm	P _y ,N	P _u ,N	F _y ,MPa	F _u ,MPa	E,MPa
1	56	12	342.217	479.017	8.5724	11.9992	724.145
2	56.56	12.14	407.974	568.281	9.88638	13.7711	715.794
3	53.42	14.4	419.436	599.945	10.5118	14.7542	687.667
4	55.37	13	510.869	727.139	11.0281	15.6967	668.442
5	55.28	12.6	349.251	543.351	8.03859	12.5061	689.662
6	56.16	11.86	386.685	512.722	9.88809	13.111	732.693

Table A-2: Sample dimensions and stress-strain responses of GFRC coupons with uncoated CemFil fibers, tested after 7 days.

Sample	b,mm	d,mm	P _y ,N	P _u ,N	F _y ,MPa	F _u ,MPa	E,MPa
1	56	14	324	331.897	5.962828	6.108163	620.6958
2	57	14	314.823	353.694	5.692288	6.395112	620.6958
3	56	14	291.208	305.868	5.359331	5.62913	615.2029
4	59	14	301.209	330.388	5.26152	5.771219	620.6958
5	56.5	14	344.961	372.458	6.292408	6.793978	620.6958

Table A-3: Sample dimensions and stress-strain responses of GFRC coupons with coated E-glass fibers, tested after 7 days.

Sample	b,mm	d,mm	P _y ,N	P _u ,N	F _y ,MPa	F _u ,MPa	E,MPa
1	53.94	13.88	334.042	453.578	6.493257	8.81685	626.062
2	60	12.88	334.235	416.537	6.782977	8.453216	674.6693
3	54.5	13.41	308.55	447.33	6.359498	9.219881	648.0045
4	55.59	13.27	347.154	472.272	7.163661	9.745521	654.8411
5	57.9	13.12	270.223	369.664	5.476807	7.492251	662.3278
6	56.34	12.83	328.565	439.643	7.15653	9.575939	677.2986

Table A-4: Sample dimensions and stress-strain responses of GFRC coupons with uncoated SIP-91 glass fibers, tested after 7 days.

Sample	b,mm	d,mm	P _y ,N	P _u ,N	F _y ,MPa	F _u ,MPa	E,MPa
1	58	14	336.111	376.759	5.97242	8.33939	620.696
2	54	13	314.963	338.345	6.97157	7.48912	668.442
3	54.5	14	272.035	291.763	5.14427	5.51733	620.696
4	60	13.5	348.795	382.079	6.44322	7.05807	643.684
5	54.5	14	287.794	320.44	5.44228	6.05962	620.696
6	60	14	264.501	286.292	4.5433	4.9176	620.696

Table A-5: Sample dimensions and stress-strain responses of GFRC coupons with uncoated SIP-115 glass fibers, tested after 7 days.

Sample	b,mm	d,mm	P _y ,N	P _u ,N	F _y ,MPa	F _u ,MPa	E,MPa
1	56.5	14	274.356	305.131	5.00451	5.56587	620.696
2	58	13	240.967	278.319	4.96586	5.73561	668.442
3	58	12.5	246.807	285.585	5.50124	6.36559	695.179
4	58	12	305.254	370.441	7.38282	8.95942	724.145
5	57.5	13	269.662	321.188	5.60553	6.67661	668.442
6	54	13	255.206	308.334	5.64887	6.82484	668.442

Table A-6: Sample dimensions and stress-strain responses of GFRC coupons with uncoated SIP-121 glass fibers, tested after 7 days.

Sample	b,mm	d,mm	P _y ,N	P _u ,N	F _y ,MPa	F _u ,MPa	E,MPa
1	54.48	14.32	208.742	288.606	3.77431	5.21835	606.825
2	55.69	13.6	249.945	313.349	4.90163	6.14504	638.952
3	46.92	13.3	193.474	223.502	4.70883	5.43966	653.364
4	54.62	13.07	207.21	239.353	4.486	5.20575	664.862
5	60.43	13.21	286.432	341.383	5.48674	6.53936	598.905
6	65.33	13.28	272.345	319.16	4.77487	5.59566	654.348

Table A-7: Sample dimensions and stress-strain responses of neat cement coupons, tested after 7 days.

Sample	b,mm	d,mm	P _y ,N	P _u ,N	F _y ,MPa	F _u ,MPa	E,MPa
1	56.41	13.56	201.938	237.016	3.932728	4.61587	640.8363
2	54.66	13.14	201.037	233.59	4.302957	4.999715	661.3197
3	59.85	12.92	177.34	202.154	3.586857	4.087375	672.3558
4	58.22	13.22	215.633	258.129	4.280865	5.124518	657.3178
5	57.08	13.23	244.725	282.708	4.947959	5.715916	656.8209
6	55.28	12.86	152.232	195.49	3.363623	4.319425	675.7186

Table A-8: Sample dimensions and stress-strain responses of GFRC coupons with coated CemFil fibers, tested after 28 days.

Sample	b,mm	d,mm	P _y ,N	P _u ,N	F _y ,MPa	F _u ,MPa	E,MPa
1	52.6	12.01	469.501	550.681	12.500176	14.66154	723.5421
2	56.37	12.69	387.936	515.364	8.6325713	11.46817	684.7707
3	63.37	14.23	334.545	428.561	5.2663826	6.746375	610.6634
4	59.31	13.38	501.481	645.685	9.5403806	12.28378	649.4575
5	56.47	12.43	452.655	578.896	10.479936	13.40269	699.0942
6	53.47	11.37	409.707	532.04	11.972742	15.54764	764.2692

Table A-9: Sample dimensions and stress-strain responses of GFRC coupons with uncoated CemFil fibers, tested after 28 days.

Sample	b,mm	d,mm	P _y ,N	P _u ,N	F _y ,MPa	F _u ,MPa	E,MPa
1	55.77	14.73	303.202	369.816	5.06148	5.95977	589.935
2	57.51	14.46	273.76	333.516	4.59877	5.60258	599.705
3	56.63	14.2	299.607	340.396	5.30005	6.02161	611.954
4	59.22	15.48	383.575	456.349	5.45998	6.49588	561.353
5	57.2	14.67	253.459	306.92	4.15913	5.0364	592.348
6	56.98	13.01	255.236	312.169	5.33764	6.53829	668.955

Table A-10: Sample dimensions and stress-strain responses of GFRC coupons with coated E-glass fibers, tested after 28 days.

Sample	b,mm	d,mm	P _y ,N	P _u ,N	F _y ,MPa	F _u ,MPa	E,MPa
1	55.83	16.19	412.247	511.354	5.69046	7.05849	536.735
2	60.38	16.21	409.756	508.881	5.21696	6.49502	536.073
3	56.57	15.76	351.525	389.847	5.05369	5.60463	551.379
4	59.24	15.89	356.26	403.788	4.81122	5.95576	546.869
5	57.28	16.26	328.202	566.896	4.37773	7.56155	534.424

Table A-11: Sample dimensions and stress-strain responses of GFRC coupons with uncoated SIP-91 glass fibers, tested after 28 days.

Sample	b,mm	d,mm	P _y ,N	P _u ,N	F _y ,MPa	F _u ,MPa	E,MPa
1	59.91	13.32	292.172	338.338	5.552419	6.429754	652.383
2	59.21	13.73	304.669	353.413	5.5137	6.39584	632.902
3	55.74	13.89	298.994	353.548	5.6162	6.64092	625.611
4	57.11	13.26	273.753	326.338	5.50695	6.56477	655.335
5	56.15	13.08	267.616	322.013	5.62728	6.15413	664.353
6	57.05	13.72	267.805	318.061	5.0374	5.98271	633.363

Table A-12: Sample dimensions and stress-strain responses of GFRC coupons with uncoated SIP-115 glass fibers, tested after 28 days.

Sample	b,mm	d,mm	P _y ,N	P _u ,N	F _y ,MPa	F _u ,MPa	E,MPa
1	52.83	14.19	249.075	315.267	4.72973	5.98666	612.385
2	59.62	14.27	301.004	351.566	5.00822	5.84949	608.952
3	58.91	12.92	251.039	303.091	5.16477	6.22602	671.54
4	58	13.1	249.245	289.454	5.05833	5.87436	663.339
5	58.35	14.35	253.991	309.317	4.26997	5.20009	605.557
6	58.62	13.89	253.932	296.51	4.53543	5.29591	625.611

Table A-12: Sample dimensions and stress-strain responses of GFRC coupons with uncoated SIP-121 glass fibers, tested after 28 days.

Sample	b,mm	d,mm	P _y ,N	P _u ,N	F _y ,MPa	F _u ,MPa	E,MPa
1	54.42	12.94	204.861	246.491	4.54134	5.46418	671.541
2	62.19	13.3	290.308	341.91	5.33073	6.27826	653.364
3	62.33	13.78	251.939	294.043	4.29983	5.01842	630.605
4	60.08	14.58	272.081	319.002	4.30333	6.29442	596.004
5	58.4	13.24	298.526	356.804	5.8904	7.04032	656.325
6	54.81	13.15	224.661	260.122	4.78815	5.54392	660.817

Table A-13: Sample dimensions and stress-strain responses of neat cement coupons, tested after 28 days.

Sample	b,mm	d,mm	P _y ,N	P _u ,N	F _y ,MPa	F _u ,MPa	E,MPa
1	56.58	12.66	238.577	270.305	5.314343	6.02109	686.3934
2	60.55	13.08	201.961	219.205	3.938123	4.274371	664.3533
3	54.45	12.77	221.274	246.175	5.033871	5.600356	680.4809
4	57.14	13.37	240.792	269.51	4.762011	5.329951	649.9432
5	58.22	13.24	253.675	288.239	5.020892	5.705004	656.3248
6	54.34	13.41	274.689	311.55	5.678262	6.440238	598.4315

Section 3

Corrosion of Glass Fibers in Cement Environments

Rossella Mafalda Ferraro¹ and Richard K. Brow²

¹Civil and Architectural Engineering

²Materials Science & Engineering Department

ABSTRACT

Glass fibers drawn from corrosion resistant iron phosphate (IP) melts were exposed to different alkaline environments and their corrosion behavior compared with commercial alkaline resistant (AR) silicate glass fibers, with and without polymer coatings. The corrosion rates, measured by sample weight losses, in aqueous alkaline environments of some IP fibers are as low as the commercial AR glasses. Uncoated IP fibers embedded for up to 28 days in a cement environment exhibit some surface corrosion, but appear otherwise unaffected.

Experimental Procedures

Glass fibers with diameters in the range 12-30 microns were drawn from platinum bushings at Mo-Sci, Inc. (Rolla, MO) from melts of iron phosphate glasses developed at UMR. Larger diameter fibers (up to 200 microns) were drawn from melt surfaces at UMR. The nominal compositions of the glasses examined in this study are shown in Table 1. In addition, commercially manufactured glass fibers were tested, including the alkali-resistant glass CemFIL¹, with and without the polymer coating used to manufacture commercial fiber.

The chemical durabilities of the alkaline-resistant commercial silicate and calcium iron phosphate glass fibers were assessed by three kinds of tests:

- *Short corrosion resistance test:* immersing fibers of selected compositions in 10 percent NaOH solution pH (~13.9) at 80°C for 24h and monitoring the pH of the solution and weight loss of the fibers. The fiber surface area-to-NaOH volume ratio during the test was ~11.4 cm⁻¹, and the fiber diameters ranged from 12 to 200µm. The fibers were periodically removed from the solution, dried in an oven at 80°C for almost an hour, then weighed to determine the weight loss (if any) as compared to the initial weight. The pH of the solution was also tested after the fiber removal to check the trend of the pH and mass loss.
- *Long corrosion resistance test:* immersing fibers of selected compositions in Lawrence Solution² at 80°C for up 2000h and monitoring the pH of the solution and weight loss of the fibers. The surface area of the powders-to-Lawrence solution volume (V) ratio during the test was ~0.21cm⁻¹. The fibers were periodically removed from the solution, dried in an oven at 80°C for almost an hour, then weighed to determine the weight loss (if any) as compared to the initial weight. The pH of the solution was also tested after the fiber removal
- *Glass fiber in Portland Cement coupons:* mixing fibers (2% by volume, 15 to 180 µm diameter) of selected composition with ordinary Portland cement and monitoring qualitatively the behavior of fiber (fiber coloration, integrity, product deposition, and fiber pull out). The coupons were stored in humid environments for up to several weeks before they were fractured and the fracture surface evaluated.

0.5g Fiber glass
25g Cement Portland
25ml Water

To make the specimen, fibers were cut with a length of about 4–5mm and put with cement and water into the polystyrene mold. Materials were then mixed by hand

¹ Cem-FIL is a registered trademark of Saint-Gobain/Vetrotex; its composition in weight % is SiO₂ 62, Na₂O 14.8, CaO 6.5, TiO₂ 0.1, ZrO₂ 16.7 and Al₂O₃ 0.8.

² 0.88g NaOH/l-H₂O, 3.45g KOH/l-H₂O, 0.48 gCa(OH)₂/l-H₂O, initial pH~13.0

using a small paddle. The mix was cast into a mold and sealed in plastic bag at room temperature (22°C) for the time needed for the evaluation. After the allotted time passed, the mold was broken, and the sample was examined by the optical microscope.

RESULTS AND CONCLUSION

Figure 1 shows the mass losses vs. time data from several different bundles of fibers held in NaOH at 80°C. Some phosphate fibers (e.g., SIP-113 and SIP-129) have chemical durabilities that are as good as the commercial CemFIL fiber; i.e., less than 1 percent weight loss in 24 hours. In general, glasses with greater CaO content and lower Fe₂O₃ content have better durability in high pH environments. (See section 1 of this report.)

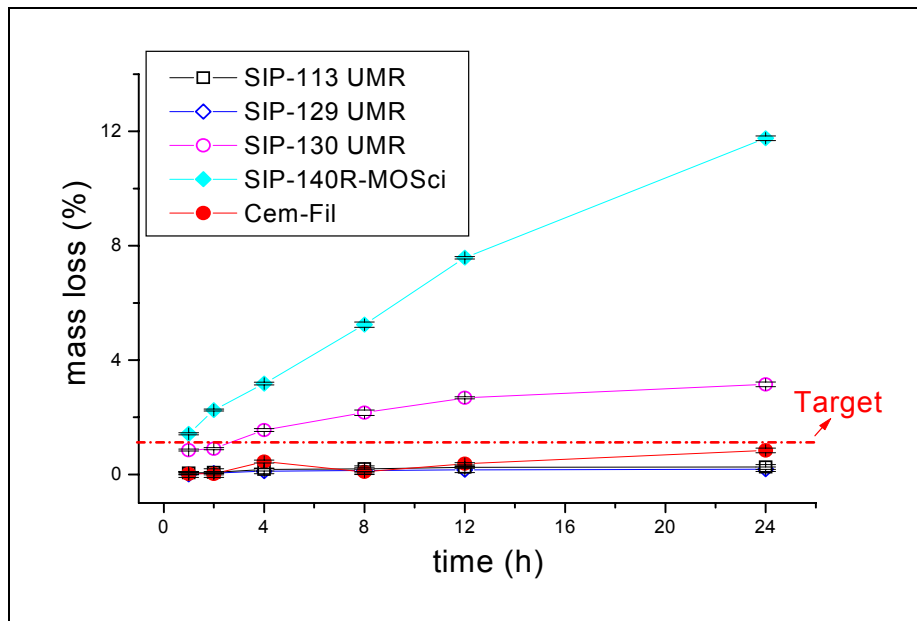


Figure 1: Uncoated glass fibers in 10 percent NaOH solution at 80°C SA:V=11.4/1 cm

Figures 2 and 3 show the weight loss of uncoated phosphate fibers in Lawrence solution for 500h at 80°C. SIP-129 has a comparable weight loss to CemFIL, and SIP-108 and 121 behave in a similar fashion to commercial E-glass fibers; uncoated basaltic fibers have weight losses that are comparable to CemFIL (figure 2). Figure 3 shows representative optical micrographs of fibers after 500 hours in Lawrence solution. A significant corrosion layer can be seen on the surfaces of the SiP-91 fibers which exhibited the greatest corrosion rates.

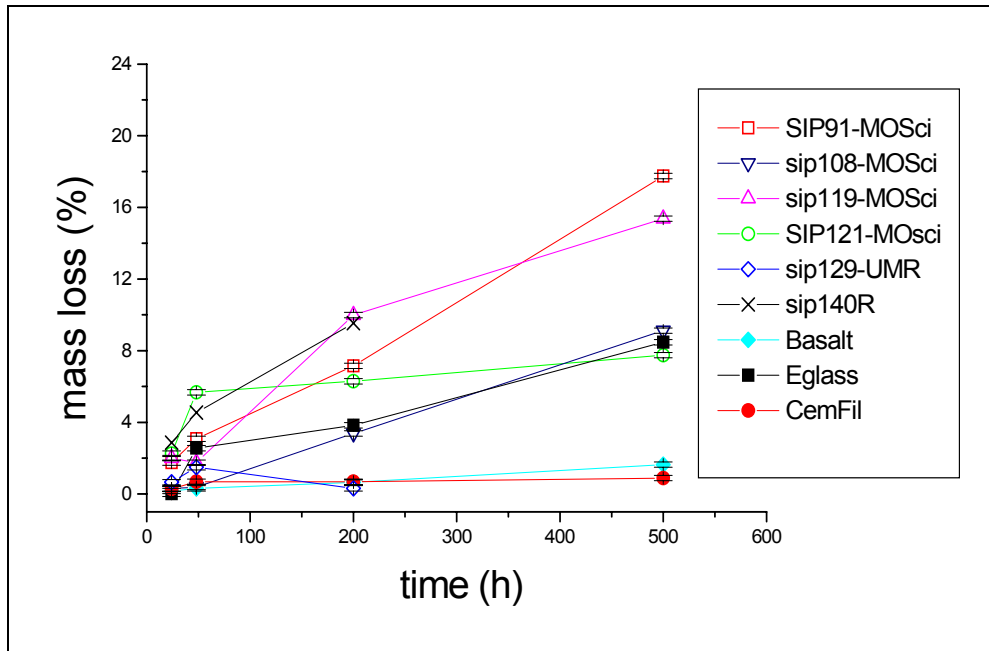


Figure 2: Uncoated glass fibers in Lawrence Solution at 80°C SA:V=11.4/1 cm

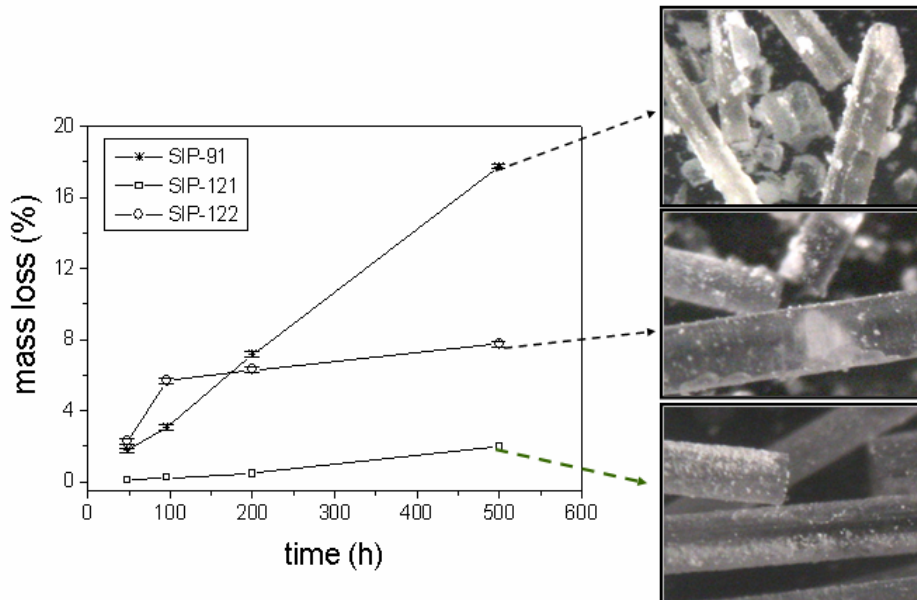


Figure 3: Weight loss (%) for uncoated phosphate glass fibers in Lawrence Solution at 80°C for 500 h; optical micrographs of representative fibers are also shown; SA:V~11.4 cm⁻¹

Table 2 summarizes the mass losses and solution pH changes for the fiber corrosion experiments in Lawrence solution after up to 500h. Several solutions exhibited significant decreases in pH and these also were associated with the largest weight losses. Figure 4 shows

optical micrographs of the surfaces of SIP-119 (left) and SIP-120 (right) fibers after test. Both show evidence for extensive surface corrosion products, consistent with the weight change measurements.

Type of Glass Fiber	Δ pH of Lawrence solution after 500 h (initial pH~13)	Mass loss (%)
Basalt (13 μ m)	-0.41	1.6
SIP108-(15 μ m)	-1.05	15.4
SIP119 (18 μ m)	-2.60	29.4
SIP120 (18 μ m)	-3.54	56.4
Cem-FIL (20 μ m)	0.46	-0.5
Cem-FIL-c (20 μ m)	-0.13	0.4
E-glass-c (20 μ m)	-0.16	3.2
SIP115 (15 μ m)	-5.20	10.8
SIP141-R	-5.05	-29.3



Figure 4: Optical micrographs of SIP-119 (left) and SIP-120 (right) fibers after 500 hour in 80°C Lawrence solution.

Representative optical micrographs of the fracture surfaces of fiber-reinforced cement composites are shown in figures 5-8. Desirable 'fiber pull-out' behavior is apparent for the Cem-FIL and SIP-129 samples. Fiber pull-out is a mechanism for increasing the flexural strength and toughness of cement matrix composites. There is little evidence for surface corrosion on the Cem-FIL and SIP-129 fibers, consistent with their performances in the alkaline solution tests. However, SIP-91 and SIP-120 are far more reactive and were difficult to find in the 28-day samples.



Figure 5: Uncoated Cem-FIL fibers in cement after 2 days (left) and after 28 days (right).

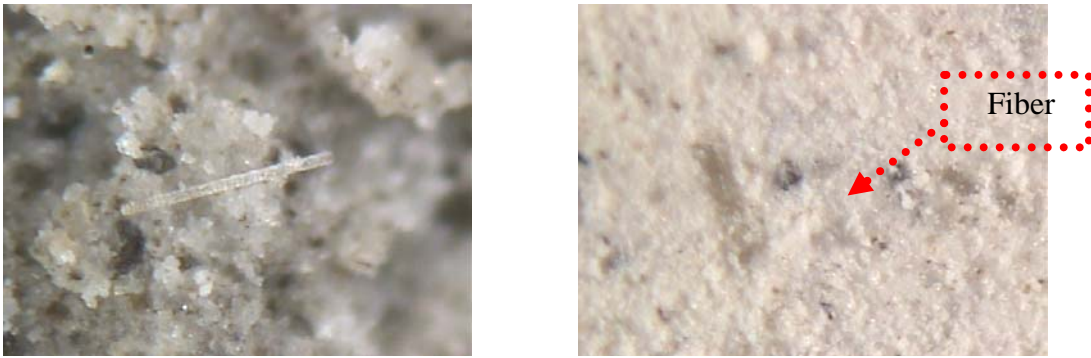


Figure 6: SIP-91 in cement after 2 days (left) and after 28 days (right)



Figure 7: SIP-120 in cement after 2 days (left) and after 28 days (right)

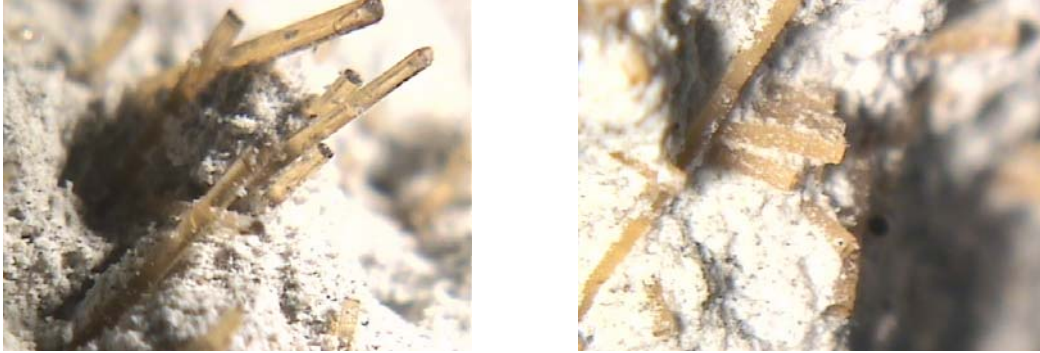


Figure 8: SIP-129 in cement after 2 days (left) and after 28 days (right)

In summary, the corrosion tests of compositionally complex phosphate glass fibers are consistent with the study of the simpler Ca-Fe-phosphate glasses (section 1), and help explain the results of the mechanical tests of the glass-fiber reinforced composites (section 2). Glasses that react more rapidly in alkaline solutions are less effective as reinforcing fibers, but even chemically stable phosphate glass compositions have limited benefit as reinforcing materials, compared with commercially-coated, alkaline resistant silicate fibers.